NAVAL POSTGRADUATE SCHOOL
Monterey, California

THESIS

PROPELLANT FEED CONTROL
FOR ION ENGINES

by

Dan A. Starling, Jr.

June 1996

Thesis Advisor: Oscar Biblarz

Approved for public release; distribution is unlimited.

REPORT DOCUMENTATION PAGE

Form Approved
OMB No. 0704-0188

1. AGENCY USE ONLY *(Leave blank)*	2. REPORT DATE	3. REPORT TYPE AND DATES COVERED
	June 1996	Master's Thesis

4. TITLE AND SUBTITLE
PROPELLANT FEED CONTROL FOR ION ENGINES

5. FUNDING NUMBERS

6. AUTHOR(S)
Starling, Dan A.

7. PERFORMING ORGANIZATION NAME(S) AND ADDRESS(ES)
Naval Postgraduate School
Monterey, CA 93943-5000

8. PERFORMING ORGANIZATION REPORT NUMBER

9. SPONSORING/MONITORING AGENCY NAME(S) AND ADDRESS(ES)

10. SPONSORING/MONITORING AGENCY REPORT NUMBER

11. SUPPLEMENTARY NOTES
The views expressed in this thesis are those of the author and do not reflect the official policy or position of the Department of Defense or the U.S. Government.

12a. DISTRIBUTION/AVAILABILITY STATEMENT
Approved for public release; distribution is unlimited.

12b. DISTRIBUTION CODE

13. ABSTRACT *(Maximum 200 words)*

An overview of space electric propulsion (SEP) is presented. Methods of throttling the power levels of electrostatic and electromagnetic thrusters are discussed. Particular attention is given to the concept of thermally-throttling propellant flow using the temperature-viscosity characteristics of xenon gas. The thermoproperties of xenon gas as a function of temperature are determined, and the flow regimes of the propellant at the mass flow rates of interest are studied. The propellant flow is presented separately as Fanno flow and as Rayleigh flow, and then those combined effects are considered. A method for predicting the performance of thermally-throttled systems is presented. Uncertainties in modeling real-world thermal throttling systems are discussed. The possible use of thermal throttling characteristics as a means of propellant pressure regulation is also examined.

14. SUBJECT TERMS	15. NUMBER OF PAGES
space electric propulsion, propellant feed, flow control, thermal throttling	86
	16. PRICE CODE

17. SECURITY CLASSIFICATION OF REPORT	18. SECURITY CLASSIFICATION OF THIS PAGE	19. SECURITY CLASSIFICATION OF ABSTRACT	20. LIMITATION OF ABSTRACT
Unclassified	Unclassified	Unclassified	UL

NSN 7540-01-280-5500

Standard Form 298 (Rev. 2-89)
Prescribed by ANSI Std. Z39-18
298-102

Approved for public release; distribution is unlimited

PROPELLANT FEED CONTROL FOR ION ENGINES

Dan A. Starling, Jr.
Lieutenant, United States Navy
B.A., University of Texas at Austin, 1989

Submitted in partial fulfillment of the
requirements for the degree of

MASTER OF SCIENCE IN ASTRONAUTICAL ENGINEERING

from the

NAVAL POSTGRADUATE SCHOOL
June 1996

Author: _____
Dan A. Starling, Jr.

Approved by: _____
Oscar Biblarz, Thesis Advisor

_____
Knox T. Millsaps, Jr., Second Reader

_____
Daniel J. Collins, Chairman
Department of Aeronautics and Astronautics

ABSTRACT

An overview of space electric propulsion (SEP) is presented. Methods of throttling the power levels of electrostatic and electromagnetic thrusters are discussed. Particular attention is given to the concept of thermally-throttling propellant flow using the temperature-viscosity characteristics of xenon gas. The thermoproperties of xenon gas as a function of temperature are determined, and the flow regimes of the propellant at the mass flow rates of interest are studied. The propellant flow is presented separately as Fanno flow and as Rayleigh flow, and then those combined effects are considered. A method for predicting the performance of thermally-throttled systems is presented. Uncertainties in modeling real-world thermal throttling systems are discussed. The possible use of thermal throttling characteristics as a means of propellant pressure regulation is also examined.

TABLE OF CONTENTS

I. INTRODUCTION

A. SPACE ELECTRIC PROPULSION

Electric propulsion devices for space applications use electrical energy (from solar cells, batteries, fuel cells, etc.) as a means to heat or to eject propellant mass, resulting in thrust. While there are several methods of electric propulsion either in use or in development, all can be described as one of three fundamental types (Sutton, 1992):

1. *Electrothermal thrusters.* Electrical energy is used to heat the propellant, which is then thermally expanded and accelerated to supersonic speeds through a nozzle, as in a typical chemical rocket.
2. *Electrostatic thrusters.* Thrust is produced by accelerating electrically charged propellant particles through an electrostatic field.
3. *Electromagnetic thrusters.* Electrical energy is used to produce a plasma (a high-temperature electrically neutral gas containing both electrons and positive ions) which interacts with electric and magnetic fields to accelerate the propellant.

The three basic subsystems of a typical space electric propulsion system are (1) a power processing unit (PPU), which contains electrical interfaces between the propulsion system and the spacecraft, and sends power and command signals to the thruster and propellant flow control signals to the propellant subsystem; (2) a propellant management assembly (PMA), which

provides a means of storing, throttling and delivering the propellant; and (3) one or more thrusters, which convert electrical energy to thrust through one of the means discussed above.

1. Electrothermal Thrusters

There are two basic types of electrothermal thrusters currently in use. The first and simplest is known as a resistojet (Figure 1), which uses electrical current to directly heat metal components such as coiled wire, tubing or fins. These components then heat the propellant through radiation and convection as it flows over them. In the example shown below, an increase of about 28% in specific impulse over a standard catalytic thruster is achieved by electrically augmenting the enthalpy of the decomposition products of hydrazine using a high-power heater in a second-stage vortex chamber; thrust results when the higher energy propellant is accelerated through the exit nozzle. Resistojet performance is limited primarily by the capacity of the

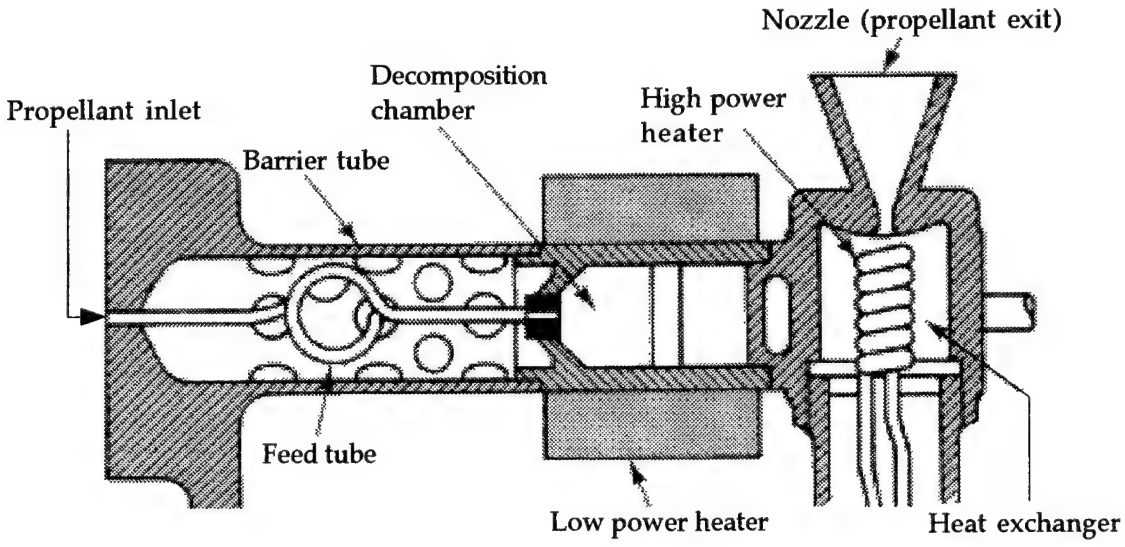

Figure 1. Resistojet thruster cross-section (From Agrawal, 1986)

thruster's structural components to withstand high temperatures. This limitation is overcome by the second basic type of electrothermal thruster, known as an arcjet. These use an attached arc within the nozzle to directly heat the propellant stream to temperatures much higher than that of the thruster body. Arcjet thrusters are limited primarily by instabilities in the arc and erosion in the nozzle.

Resistojets can produce thrust levels of 300–500 mN at a specific impulse of about 300 seconds and an efficiency of 65–90%. Arcjets can produce thrust levels of 200–700 mN at a specific impulse of 400–1600 seconds and an efficiency of 40–65%. Electrothermal thrusters have been flight-tested on a number of spacecraft, including Intelsat V. NASA currently has two electrothermal thrusters under development: a 600 s I_{sp}, 2 kW arcjet for commercial communications satellite north-south stationkeeping, and a 500 s I_{sp} low power arcjet thruster (LPAT). The U.S. Air Force currently has both 30 kW and 1 kW arcjet thrusters under development.

2. Electrostatic Thrusters

Electrostatic thrusters use electrostatic fields to accelerate charged particles in a linear direction, producing thrust. While electrons are relatively easy to produce, their small mass makes them impractical for use as a propellant. Accordingly, electrostatic thrusters use heavy atoms charged as positive ions (since neutralization with electrons is practical) or charged colloids (liquid droplets). These thrusters can be categorized by their source of charged particles as follows (Sutton, 1992):

1. *Electron bombardment thrusters.* Positive ions are produced by bombarding vaporized or gaseous propellant (such as xenon or mercury) with electrons emitted from a heated cathode (Figure 2).
2. *Ion contact thrusters.* Positive ions are produced by passing propellant vapor (usually cesium) through a hot contact ionizer (usually tungsten).
3. *Field emission (colloid) thrusters.* Tiny liquid droplets of propellant are charged by passing them through a corona discharge.

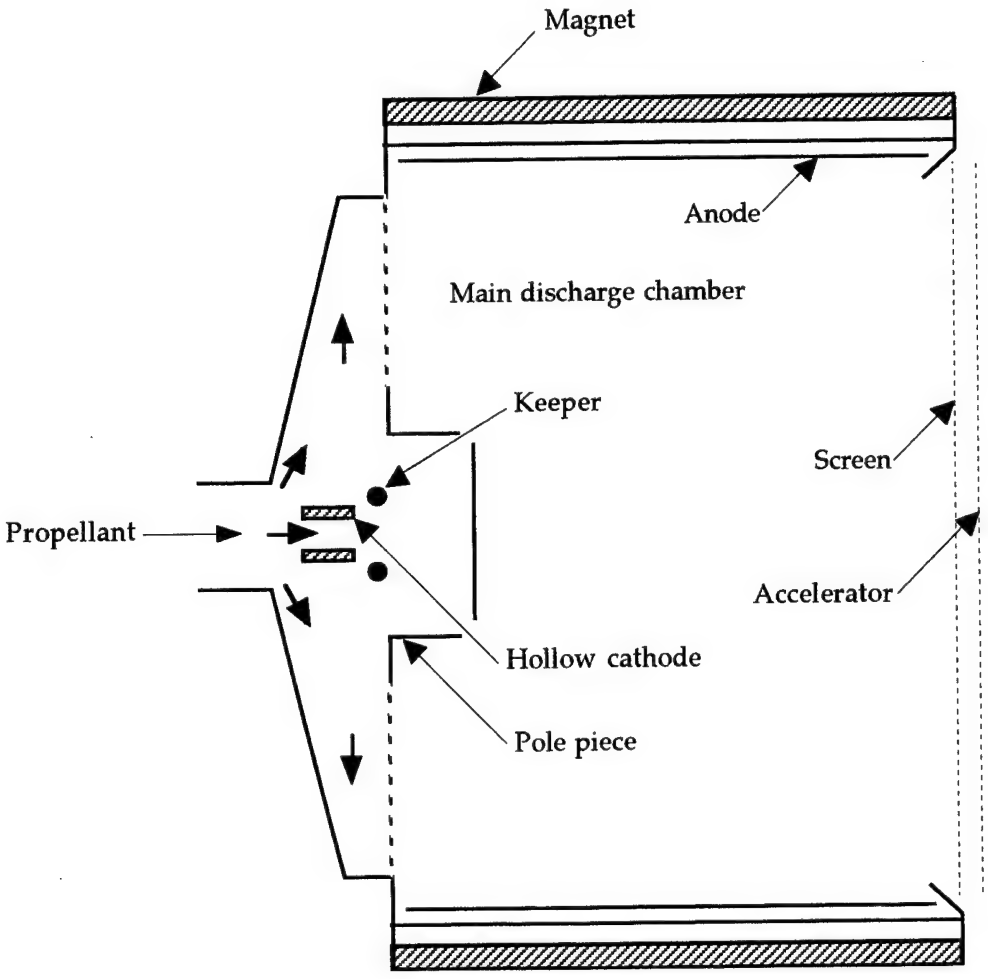

Figure 2. Electron bombardment ion thruster (From Agrawal, 1986)

Electron bombardment ion thrusters can produce thrust levels of up to 100 mN at a specific impulse of as much as 5000 seconds and an efficiency of 50–65%. Ion contact thrusters can produce thrust levels of up to 500 mN at a specific impulse of as much as 5000 seconds and an efficiency as high as 90%. Field emission thrusters can produce thrust levels of up to 200 mN at a specific impulse of 4000–6000 seconds and an efficiency of more than 95%. There are currently no U.S. development efforts directed toward either ion contact thrusters or field emission thrusters. Electron bombardment thrusters have, however, been flight-tested on a number of U.S. spacecraft, and there are several programs pursuing further development of these thrusters in the United States. Chief among these, NASA is currently developing a 30-centimeter xenon ion engine for the NSTAR (NASA Solar Electric Propulsion Technology Application Readiness) program, which will serve as the powerplant for the New Millennium spacecraft scheduled for launch beginning in 1998. The U.S. Air Force Office of Scientific Research (AFOSR) is also involved in electrostatic thruster development, funding research of a variant which would use C60 (Buckminsterfullerene) as a propellant. Heavy particles such as this are desirable in electrostatic thrusters, where the thrust per unit area increases as the square of the particle mass to charge ratio; such particles contribute the desirable operating characteristic of high voltage and low current.

3. Electromagnetic Thrusters

Electromagnetic thrusters (also known as magnetoplasma-dynamic or MPD thrusters) differ from electrostatic thrusters in that these utilize

propellant gas that has been heated to a plasma state. There are several variations on this type of thruster, each of which requires its own unique and complex analytical model. Most, however, use plasma as part of a current-carrying electrical circuit which interacts with a magnetic field to produce thrust.

Among the most interesting of the electromagnetic thrusters (and the focus of much of this report) are those known as Stationary Plasma Thrusters (SPTs), the design of which results in an electric field which is largely axial and points in the direction of the propellant flow, serving in turn to accelerate the ions in the exhaust to velocities as high as 16,000 meters per second, for a specific impulse of more than 1600 seconds (Brophy, 1992). Figure 3 shows a schematic diagram of an SPT.

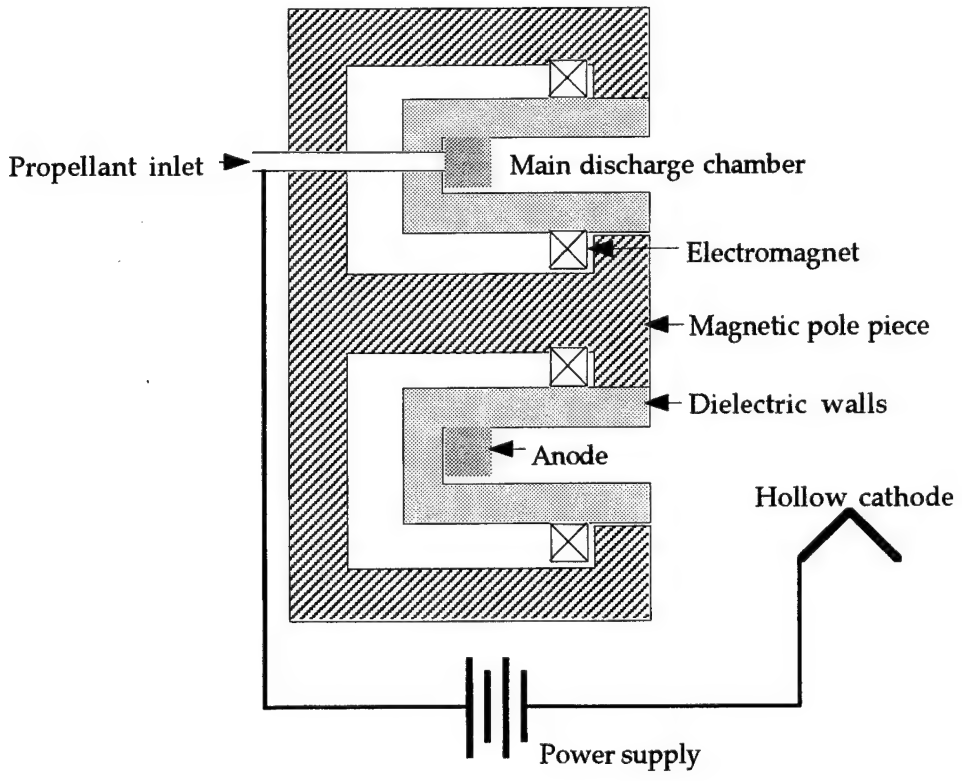

Figure 3. Stationary plasma thruster schematic diagram (After Brophy, 1992)

Stationary plasma thrusters are often referred to as Hall thrusters or Hall accelerators, after the closed circular electron drift they exhibit between the cathode and anode, which is analogous to the Hall effect. Work on Hall accelerators originated in the United States in 1962 (Figures 4 and 5). However, U.S. research in this area had effectively ceased by 1970. By contrast, the former Soviet Union (present-day Russia) have employed stationary plasma thrusters for space applications since 1964, and their successes led to a reemergence of U.S. interest in the technology by the end of the last decade.

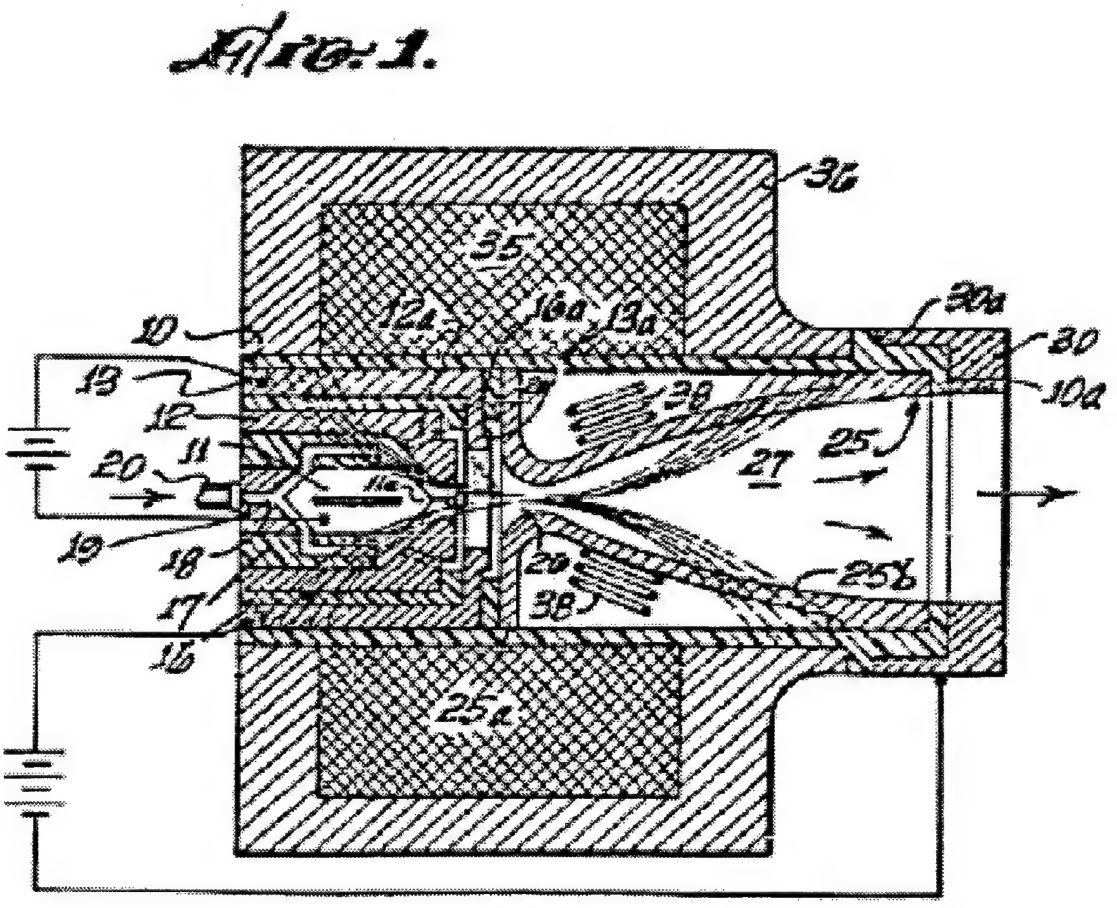

Figure 4. Plasma accelerator using Hall currents (From Cann, 1962)

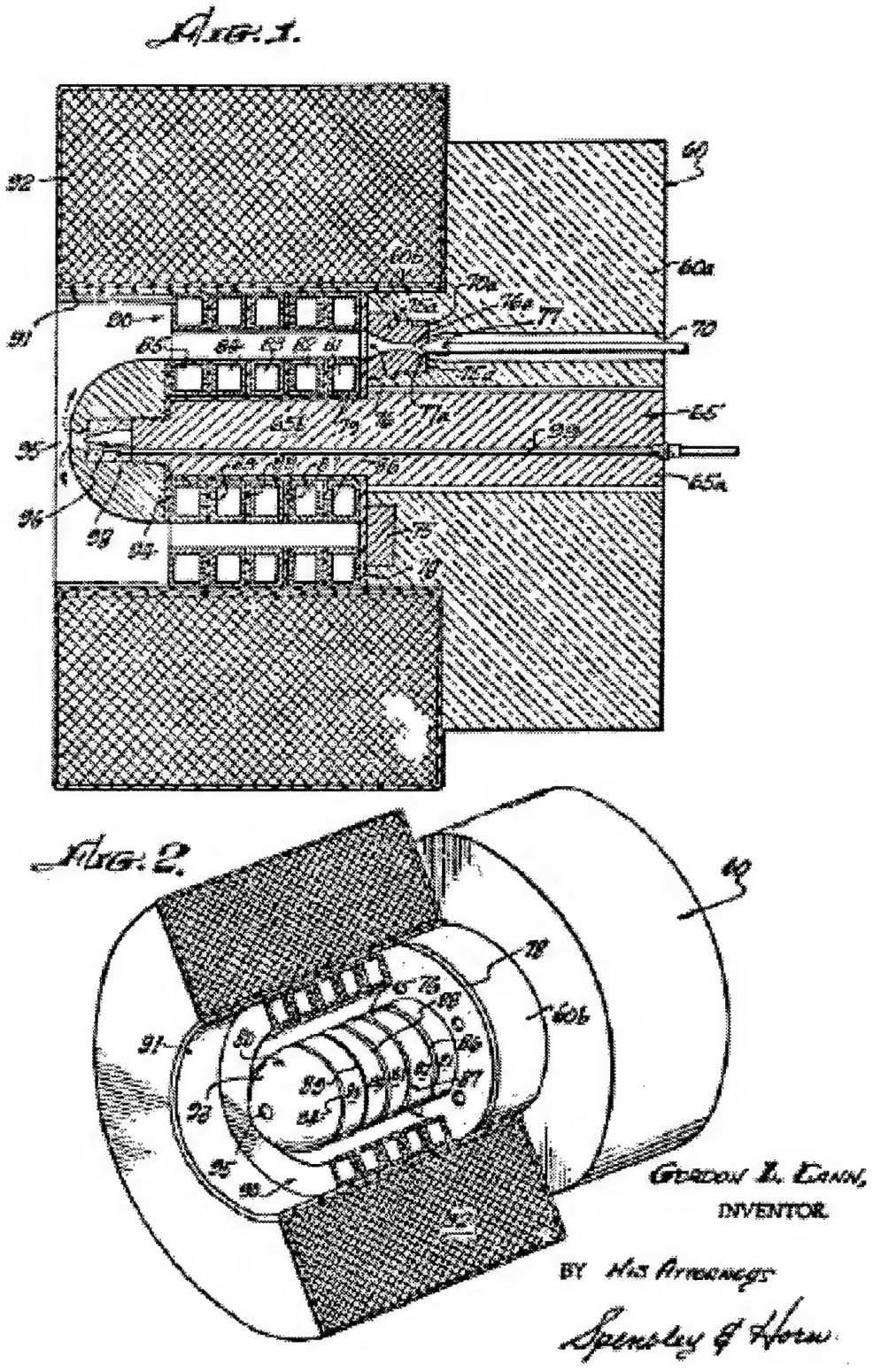

Figure 5. Annular magnetic Hall current accelerator (From Cann, 1964)

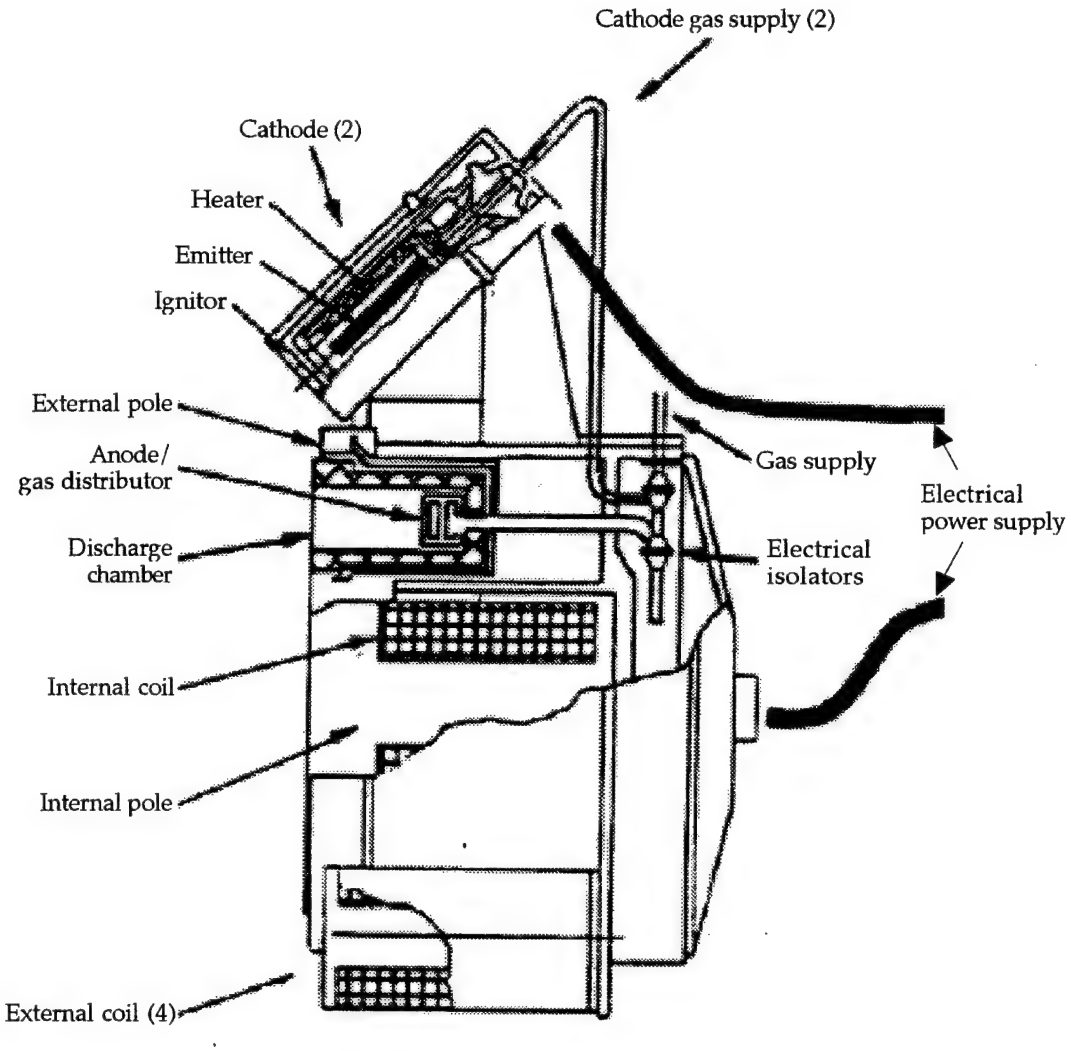

Figure 6. Stationary plasma thruster cross-section (From Day, 1995)

In 1991, a team of U.S. electric propulsion specialists visited Russia to experimentally evaluate the performance of a 1.35 kW stationary plasma thruster, designated the SPT-100 (Figure 6). Their examination verified that the actual performance of the thruster was close to the claimed performance: a thrust level of 80 mN at a specific impulse of 1600 seconds and an efficiency of 50%. Since that time, several SPT-100 thrusters have been made available to the United States for continued research and development at NASA's

Lewis Research Center and Jet Propulsion Laboratory. Additionally, Space Systems/Loral is currently flight-qualifying SPT-100 thrusters for north-south stationkeeping and orbit-raising applications on their satellites.

B. ION ENGINE POWER THROTTLING

Xenon ion propulsion systems have been proposed for use aboard interplanetary missions in the future, and NASA's NSTAR program will test the concept. Since the electrical power available to the thruster from solar energy will decrease with the square of the distance from the sun, these systems will have to be capable of power throttling across a wide range of inputs, a requirement that has not existed in the stationkeeping roles for which ion engines have been previously used. Accordingly, there is considerable interest in methods of throttling the output power of ion thrusters. Gridded ion thrusters such as NASA's 30-centimeter NSTAR engine may be throttled by varying discharge chamber voltage and current. These and Hall thrusters as well may also be throttled by varying the flow rate of the xenon gas propellant. It is this latter method which will be considered in detail in the rest of this report.

II. OVERVIEW OF CURRENT PROGRAMS

A. NASA–JET PROPULSION LABORATORY ION PROPULSION INITIATIVES

1. NSTAR 30-Centimeter Ion Engine

The NSTAR program was established in 1993 as a means to assess the baseline capabilities of ion engine technology and confirm its potential to serve as a primary space propulsion system (Curran, 1995). The program is managed by the Jet Propulsion Laboratory, with NASA's Lewis Research Center responsible for developing the 30-centimeter xenon ion engine which has become the program's focus. Hughes Corporation is the prime contractor for the majority of the flight hardware, with the notable exception of the propellant feed system, which has been developed by Moog, Incorporated.

NSTAR's electrostatic engine will provide the main propulsion system for NASA's New Millennium series of interplanetary missions, with the first launch scheduled for 1998. The 30-centimeter engine is considered ideal for these missions for a number of reasons. First, the engine itself is somewhat modular, allowing a spacecraft to use a main propulsion bank consisting of six hexagonally-arranged engines operating as a single unit (Figure 7). As higher power ion thrusters are developed, this arrangement is expected to eventually result in a segmented ion engine capable of power levels as high as 100 kilowatts, and specific impulses approaching 10,000 seconds, literally an order of magnitude greater than anything yet flown (Brophy, 1992). Second, the NSTAR engine is capable of being throttled across a wide range of output

powers, from 0.5 to 2.5 kW at efficiencies of 55–63%. This capability will allow the engine to vary its operation according to changes in the spacecraft's distance from the sun.

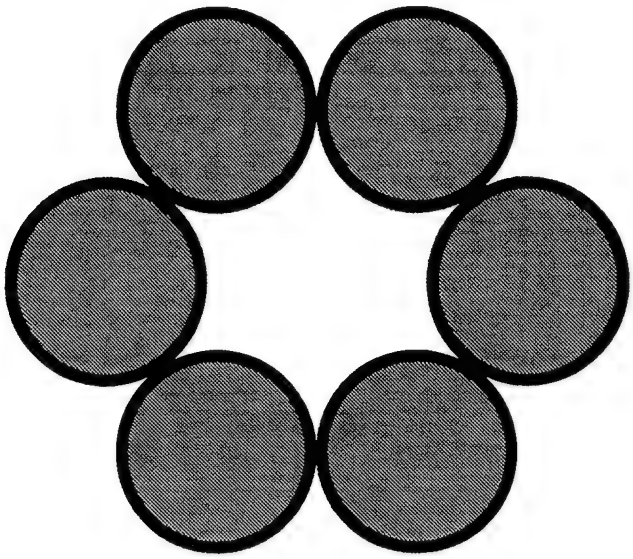

Figure 7. Segmented Ion Thruster Arrangement (End View)

2. Stationary Plasma Thruster

As mentioned previously, the type of electromagnetic ion engine known as the stationary plasma thruster (SPT) was primarily developed in the former Soviet Union; in fact, these engines are often referred to as Russian Hall thrusters (RHTs). Since 1993, development of a 100-centimeter stationary plasma thruster, the SPT-100, has taken place under a joint venture, International Space Technology, Inc. (ISTI), founded by Space Systems/Loral, the Russian Experimental Design Bureau Fakel and the Research Institute of Applied Mechanics and Electrodynamics (RIAME).

Performance, plume and EMI/RFI tests were performed on the SPT-100 at NASA's Lewis Research Center in 1993, and a 5,730-hour endurance test was completed at the Jet Propulsion Laboratory in November, 1994 (Garner, 1995). The SPT-100 thruster body and xenon flow controller (XFC) are manufactured by Fakel. The thruster's power processing unit (PPU) was developed and is manufactured by Space Systems/Loral, while the SPT-100's propellant management assembly (PMA) is built by Moog, Inc.

Stationary plasma thrusters produce a specific impulse of about 1600 seconds at an efficiency of more than 50%, and have demonstrated lifetimes in excess of 6000 hours. These characteristics make them ideal for north-south stationkeeping roles on geostationary spacecraft. Like the NSTAR engine, they may also prove to be suitable as main propulsion engines for interplanetary missions. Although stationary plasma thrusters have an extensive flight history on Russian spacecraft, their flight-qualification on western spacecraft has been delayed because of the need to redesign their PPU using western components and design practices in order to reduce subsystem mass and increase reliability (Day, 1995).

One particularly unique feature included as part of the xenon flow controller on Fakel-built stationary plasma thrusters is an integrated "thermothrottle" used for fine control of the thruster's propellant flow rate. The thermothrottle is a capillary tube flow control device which exploits the viscosity variation of xenon gas with temperature (Day, 1995). Chapters III and IV of this report will explore the concept of thermally throttling propellant flow in much greater detail.

B. ION ENGINE LIMITATIONS

Ion engines require an external source of electrical power, which is used to ionize and accelerate, and then to neutralize, the propellant. Thrust is produced only by propellant acceleration; the ionization and neutralization processes represent losses amounting to more than one-third of the input power. Other power losses may result from incomplete propellant ionization or premature neutralization, exhaust dispersion, and component heating.

The power conditioning subsystem for an ion engine must typically provide outputs at two or three different grid voltages, two different cathodes and their heaters, and two or more electromagnets, as well as actuating power for isolation valves (Sutton, 1992). In some cases, ion engine PPUs have required over 4000 discrete parts and twelve power supplies in order to operate the thruster (Hamley, 1995); these PPUs can weigh more than the thrusters themselves, and can be more difficult to flight-qualify.

The relatively low thrust levels produced by ion engines (typically less than 0.1 N) require that the thrusters operate for long periods of time in order to produce desired velocity changes. For example, using an ion propulsion system to raise a satellite from low earth orbit to geostationary orbit could require continuous thruster operation for as long as 200 days. Ion engines selected for interplanetary missions will be required to operate continuously and reliably for years without maintenance, a capability they have not yet demonstrated (Sutton, 1992).

The need for reliable and wide-ranging power throttling of ion engines, especially those used in interplanetary roles, imposes additional constraints on the thruster's power processing unit, which must be able to vary several of

the outputs mentioned above across the thruster's entire operating range. Power throttling also imposes additional requirements on the engine's xenon flow controller and propellant management assemblies, since the most commonly employed method of power throttling ion engines is to vary the thruster's propellant flow rate.

C. THESIS OBJECTIVES

The thermothrottle device employed on Fakel-built Russian Hall thrusters represents a simple and lightweight means of throttling thruster propellant flow, since the device itself consists of little more than a capillary tube through which an electric current flows. However, current RHTs use the thermothrottle for only fine control of propellant flow, and the devices as currently employed require sophisticated propellant management assemblies to maintain propellant feed pressure within narrow limits. It is believed that the thermothrottle concept may, in an expanded role, offer much greater throttling capabilities for both the stationary plasma thruster and the NSTAR ion engine, and so may allow for future reductions in the complexity of both the power processing unit and propellant management assembly. The goal of this report, then, is to assess the theoretical capabilities and limitations of thermally throttling xenon propellant flow across a wide range of both flow rates and input pressures, and to explore ways in which thermal throttling may be used to reduce constraints on the PPU and PMA.

III. THEORETICAL BACKGROUND

A. XENON PROPELLANT

1. Advantages and Disadvantages

The most desirable ion engine propellant would have a large atomic mass (which increases thrust); would be inert, inexpensive and easy to store and ionize; and would exist in a gaseous state throughout the propulsion system's storage and operating temperature ranges. Early ion engines used cesium or mercury as propellants; however, these elements have largely been abandoned due to their toxicity. Xenon, the noble gas with the highest atomic mass, is currently the preferred propellant for ion engines, although several argon-propelled systems are also under development. Rare and relatively expensive, xenon exhibits nearly ideal ion propulsion characteristics in every other aspect. A monatomic gas at room temperature, xenon is inert and easily ionized, and can be stored for years at moderate pressures without degradation.

2. Thermoproperties

Xenon exhibits essentially constant values of specific heat, gas constant and specific heat ratio. The other primary thermoproperties of gaseous xenon (enthalpy, entropy function, internal energy, thermal conductivity, sonic speed and viscosity) are functions only of temperature. Most significant to the

concept of thermally throttling xenon flow is the variation of the element's viscosity with temperature, which can be accurately calculated according to the following polynomial fit (Biblarz, 1981):

$$\mu = 1.8918 \times 10^{-6} + 6.0506 \times 10^{-8} T + 8.1794 \times 10^{-11} T^2 - 2.0510 \times 10^{-13} T^3 + 2.0165 \times 10^{-16} T^4 - 9.5234 \times 10^{-20} T^5 + 1.7663 \times 10^{-23} T^6 \quad (3.1)$$

Equations for the specific heat, gas constant, specific heat ratio, enthalpy, entropy function, internal energy, thermal conductivity, sonic speed and viscosity of xenon are given in Appendix A, as is MATLAB code for calculating the thermoproperties of xenon over a range of temperatures. Those properties are tabulated in Table A-1.

B. FLOW REGIMES

As described by Gombosi in his recent work on gas kinetics (1994), viscous gas flow falls into three different regimes: collision-dominated (Poiseuille) flow, collisionless (free molecular) flow, and intermediate (transition or slip) flow. The different regimes can be characterized by the related dimensionless parameters of Mach number (M), Knudsen number (Kn) and Reynolds number (Re). The Mach number (Equation 3.2) is defined as the ratio is the bulk flow speed of the gas (v) to its sonic speed (a). The Knudsen number (Equation 3.3) is defined as the ratio of the mean free path separating collisions between molecules (λ) and a characteristic linear size of the problem (L). The Reynolds number (Equation 3.4), which is defined as the ratio of the bulk momentum flux ($Lv\rho$) and the viscosity of the gas (μ), can also be expressed (Equation 3.5) in terms of the Mach and Knudsen numbers.

$$M = \frac{v}{a} \tag{3.2}$$

$$Kn = \frac{\lambda}{L} \tag{3.3}$$

$$Re = \frac{Lv\rho}{\mu} \tag{3.4}$$

$$Re = 3\sqrt{\gamma\frac{\pi}{8}}\frac{M}{Kn} = 1.88\sqrt{\gamma}\frac{M}{Kn} \tag{3.5}$$

The Knudsen number has been found to be a good indicator of the collisional flow regime of a given problem (Gombosi, 1994). When $Kn \ll 1$ (i.e., the mean free path is very small compared to the characteristic length of the problem), molecules undergo a large number of collisions while traveling any distances comparable to the scale of the problem, and the flow is collision-dominated. The collision-dominated regime can be easily analyzed using the methods of classical compressible fluid dynamics. This analysis can be further simplified if the flow velocity is small (the Reynolds number is less than about 2000), in which case the flow of the gas is considered to be laminar and is primarily controlled by its viscosity.

At the other extreme, when $Kn \gg 1$, the effects of intermolecular collisions are negligible and the flow is said to be collisionless. In this regime, molecules will collide with the walls of their container, but their collisions with each other may be ignored. Mathematical methods for the analysis of free molecular flow have been extensively developed in recent years.

The intermediate regime, when $Kn \approx 1$, is mathematically the most difficult to describe and has been the least studied of the three flow regimes. There are currently no well-developed standard techniques for the general analysis of a transition flow problem.

In the case of a propellant feed system using xenon gas at a pressure of two atmospheres and a temperature of 300 K, the mean free path is on the order of 10^{-8} meters. With a characteristic problem length of about 3 millimeters (the inside diameter of the tubing used in a typical system), a Knudsen number of about 10^{-6} results, indicating that the problem is certainly one involving collision-dominated flow. Furthermore, it will be shown later that at the mass flow rates of interest (1–6 mg/sec), the gas velocity is low enough that the flow is entirely laminar and is therefore dominated by viscosity and temperature effects.

Appendix B provides equations and MATLAB code relating isentropic flow properties to Mach number. These isentropic flow parameters are tabulated in Table B-1.

C. FLOW DYNAMICS

1. Fanno Flow

Fanno flow is the adiabatic flow with friction of a compressible fluid in a constant-area duct. [Note: There are numerous outstanding texts which cover all aspects of Fanno flow and, as is considered in the next section, Rayleigh flow. The author relied primarily on Zucrow (1976) and Shapiro (1953) throughout this discussion of flow dynamics.] Since it is flow in which

friction alone is the driving force affecting the thermodynamic states of the fluid, Fanno flow is also referred to as simple frictional flow. Fanno flow is related to the bulk properties of the fluid through a friction coefficient *f*; in the case of laminar flow, the D'Arcy friction factor is a function only of the Reynolds number:

$$f = \frac{64}{Re} \tag{3.6}$$

Equation 3.6 is valid when the Reynolds number is less than about 2000, so it is useful at this point to confirm that this is in fact the case. Using the continuity equation for mass flow rate and the fact that the characteristic length of propellant feed problems like the ones to be considered in this report is equal to the diameter of the feed tubing, Equation 3.3 can be rewritten as follows:

$$Re = \frac{\dot{m}}{A}\frac{D}{\mu} = \frac{4}{\pi D^2}\frac{\dot{m}D}{\mu} = \frac{4}{\pi}\frac{\dot{m}}{\mu D} \tag{3.7}$$

Using the limiting values of the maximum mass flow rate of interest (6 mg/sec) and (from Appendix A) the minimum xenon viscosity (which will occur at the minimum temperature of interest, 275 K), Equation 3.7 yields a maximum possible Reynolds number of 116, well below 2000. Accordingly, the gas flows of interest are all laminar, and Equation 3.6 is valid as a means of determining the friction factor.

A plot of enthalpy (h) as a function of entropy (s) for a constant value of mass flux ($G=\rho v$) for the case of adiabatic constant-area flow with friction is called a Fanno line; such a plot is given in Figure 8. The Fanno line can be

divided into upper (subsonic) and lower (supersonic) branches, which, in the case of increasing frictional effects (either by increasing f or duct length, or decreasing duct diameter), converge at the maximum entropy point at the right. At this point, the flow velocity becomes sonic (M=1), and the flow is said to be choked. In other words, if the initial fluid velocity is subsonic (as is the case with propellant feed systems), increasing the effects of friction accelerates the fluid flow to sonic speed as a limit. Continuing to increase the frictional effects once the sonic limit has been reached will have the effect of causing the flow to move along a new Fanno line at a lower flow rate.

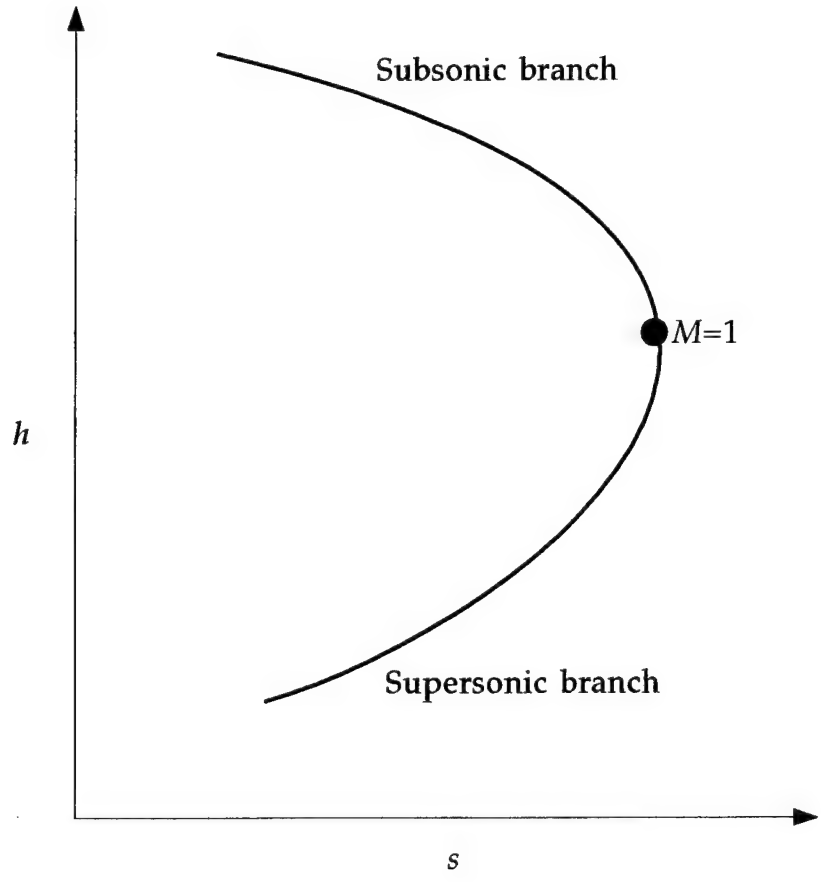

Figure 8. A Fanno line in the h-s plane.

Appendix C provides equations relating Fanno flow properties to Mach number, along with MATLAB code used to calculate fluid properties over a range of Mach numbers. These Fanno flow parameters are tabulated in Table C-1. Appendix D provides the same information for the special case of isothermal Fanno flow.

2. Rayleigh Flow

Ideal Rayleigh flow is the frictionless flow with heat transfer of a compressible fluid in a constant-area duct. Since in this case heat transfer alone is the driving force affecting the thermodynamic states of the fluid, Rayleigh flow is also occasionally referred to as simple diabatic flow. The assumption that Rayleigh flow is frictionless is particularly valid in cases where the heat transfer is accomplished in such a short length of duct that the effects of friction can be considered negligible, as is likely to be the case with a thermal throttling system. The effect of Rayleigh flow on a fluid's bulk properties is normally determined through the use of basic heat transfer equations to determine changes in the stagnation temperature of the fluid; gas dynamics relations are then used to determine changes in the other thermodynamic properties of the fluid.

As with Fanno flow, it is instructive to plot enthalpy (h) as a function of entropy (s) for a constant value of mass flux ($G=\rho v$) for the case of simple diabatic flow, producing a Rayleigh line such as is shown in Figure 9. The Rayleigh line too can be divided into upper (subsonic) and lower (supersonic) branches, which, in the case of increasing stagnation temperature, converge at the maximum entropy point at the right. At this point, the flow velocity

becomes sonic (M=1), and the flow may be considered to be thermally choked. Similarly to the case with Fanno flow, continuing to add heat once the limiting case has been reached has the effect of moving the flow to a new Rayleigh line at a lower flow rate.

Appendix E provides equations relating Rayleigh flow properties to Mach number, along with MATLAB code used to calculate fluid properties over a range of Mach numbers. These Rayleigh flow parameters are tabulated in Table E-1.

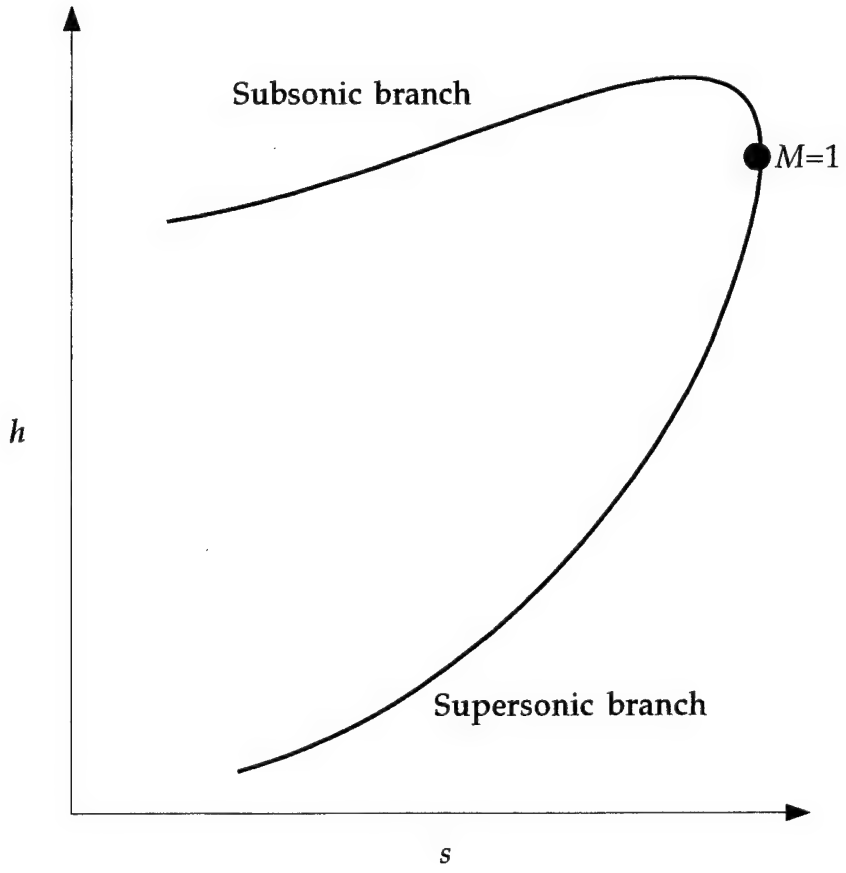

Figure 9. A Rayleigh line in the h-s plane.

3. Combined Effects of Friction and Heat Transfer

Fanno flow assumes that there is no (or negligible) heat transfer, while Rayleigh flow assumes the same regarding friction; it may seem at first that the two are mutually exclusive. In the design of a thermally-throttled propellant feed system, however, it is necessary to consider the case where both heat transfer and friction are present. Shapiro (1953) presents a set of influence coefficients which relate the combined effects of changing area, friction and temperature on the Mach number of a flowing fluid:

$$\frac{dM^2}{M^2} = -\frac{2\left[1+\frac{\gamma-1}{2}M^2\right]}{1-M^2}\frac{dA}{A} \qquad \text{[area change]}$$

$$+\frac{\gamma M^2\left[1+\frac{\gamma-1}{2}M^2\right]}{1-M^2}f\frac{dx}{D} \qquad \text{[friction]}$$

$$+\frac{\left(1+\gamma M^2\right)\left[1+\frac{\gamma-1}{2}M^2\right]}{1-M^2}\frac{dT_t}{T_t} \qquad \text{[heating / cooling]} \qquad (3.8)$$

Equation 3.8 shows that in the case of a constant-area feed system, provided that the heat transfer takes place within a relatively short length of tubing (the actual thermal throttle), it is reasonable to consider the effects of the heat transfer separately from those of the friction. In other words, by maximizing dT within a minimum dx (with dA=0), we can assume that only heat transfer affects the fluid within the thermal throttle itself. In all other sections of the feed system, both dT and dA are assumed to be zero or negligible, and the only effect is from friction. Figure 10 illustrates the Fanno (1→2)-Rayleigh (2→3)-Fanno (3→4) transitions such a system would exhibit.

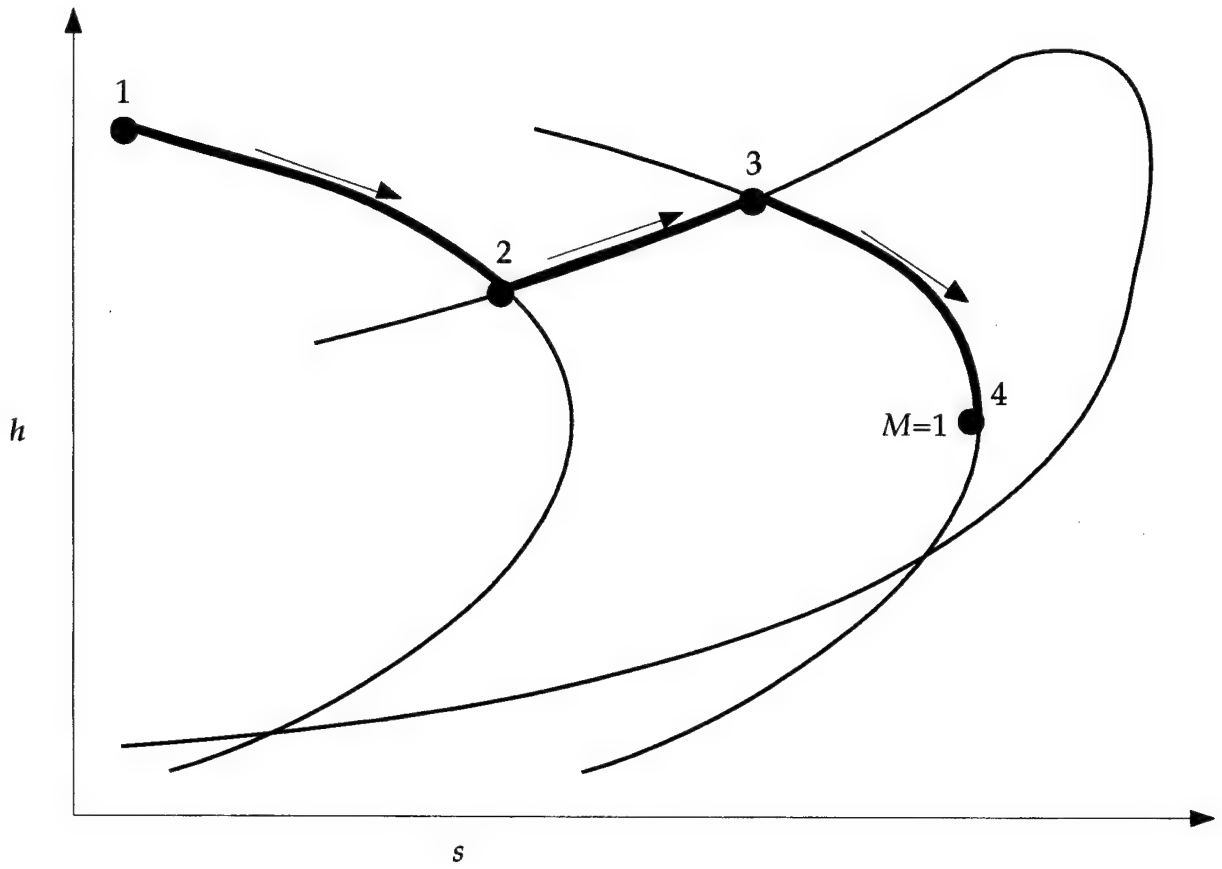

Figure 10. Combined Fanno and Rayleigh Effects

IV. ANALYSIS

A. TEMPERATURE EFFECTS ON XENON FLOW

1. Viscosity

Recall from Equation 3.1 that the viscosity of xenon as a function of temperature (in the range of 120–1500 K) is given by:

$$\mu = 1.8918 \times 10^{-6} + 6.0506 \times 10^{-8} T + 8.1794 \times 10^{-11} T^2 - 2.0510 \times 10^{-13} T^3 + 2.0165 \times 10^{-16} T^4 - 9.5234 \times 10^{-20} T^5 + 1.7663 \times 10^{-23} T^6 \quad (3.1)$$

Figure 11 shows a plot of xenon viscosity vs. temperature; note from the detailed inset figure that in the temperature range of interest (275–375 K), xenon viscosity is essentially linear, and can be estimated from:

$$\mu = [2.146 + 0.00714(T - 275)] \times 10^{-5} \quad \left[\frac{\text{N} \cdot \text{sec}}{\text{m}^2}\right] \quad (4.1)$$

2. Reynolds Number

Equation 3.7 gave the Reynolds number in terms of mass flow rate, viscosity and tubing diameter. Combining Equation 3.7 with Equation 4.1, and assuming a typical tubing diameter of 3 millimeters, the Reynolds number can be expressed in terms of mass flow rate and temperature alone:

$$Re = \frac{4 \times 10^8}{3\pi} \frac{\dot{m}}{2.146 + 0.00714(T - 275)} \quad (4.2)$$

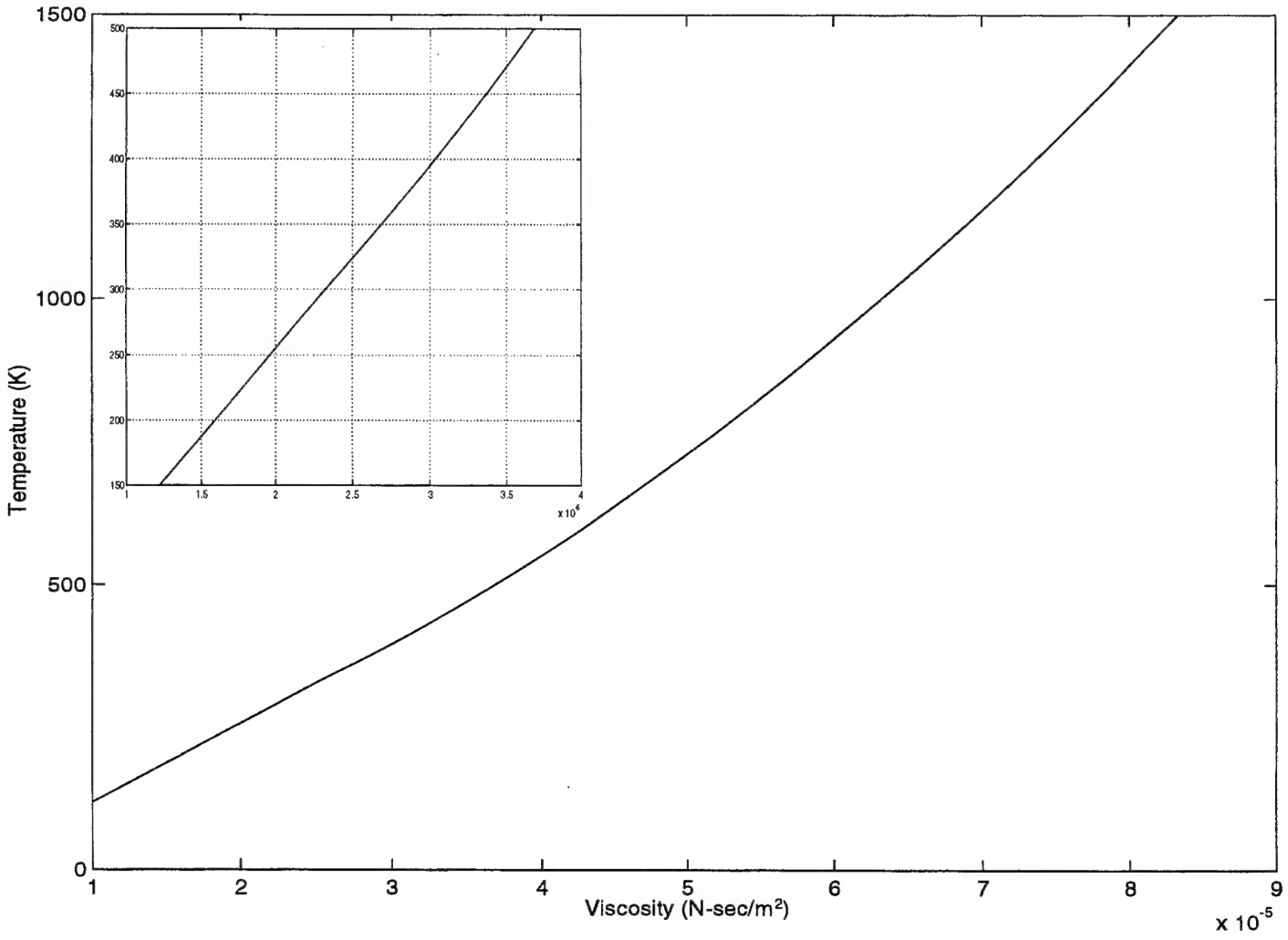

Figure 11. Xenon viscosity as a function of temperature.

Figure 12 shows the Reynolds number as a function of temperature determined using Equation 4.2 for several mass flow rates in the range of interest for propellant feed systems.

3. D'Arcy Friction Coefficient

Equation 3.6, which gave the D'Arcy friction factor as a function of the Reynolds number for laminar flow, can be combined with Equation 4.2 to relate the friction factor to temperature and mass flow rate:

$$f = \frac{48\pi}{10^8} \frac{2.146 + 0.00714\,(T - 275)}{\dot{m}} \tag{4.3}$$

Figure 13 presents the D'Arcy friction factor as a function of xenon temperature for several mass flow rates of interest. (Note: several texts use the Fanning friction coefficient, which is equal to $f/4$, instead.)

4. Mass Flow Rate

Temperature effects on the flow of xenon occur as a result of changes in the friction factor. The effect of friction varies directly with the length and inversely with the diameter of the duct. Tables of Fanno flow parameters (such as Table C-1) account for these variations by including the length-to-diameter ratio in their calculations, which result in a critical length parameter $4fL/D$. The effect of friction (and therefore temperature) can be seen by comparing isentropic choking flow to frictional choking flow, as a function of

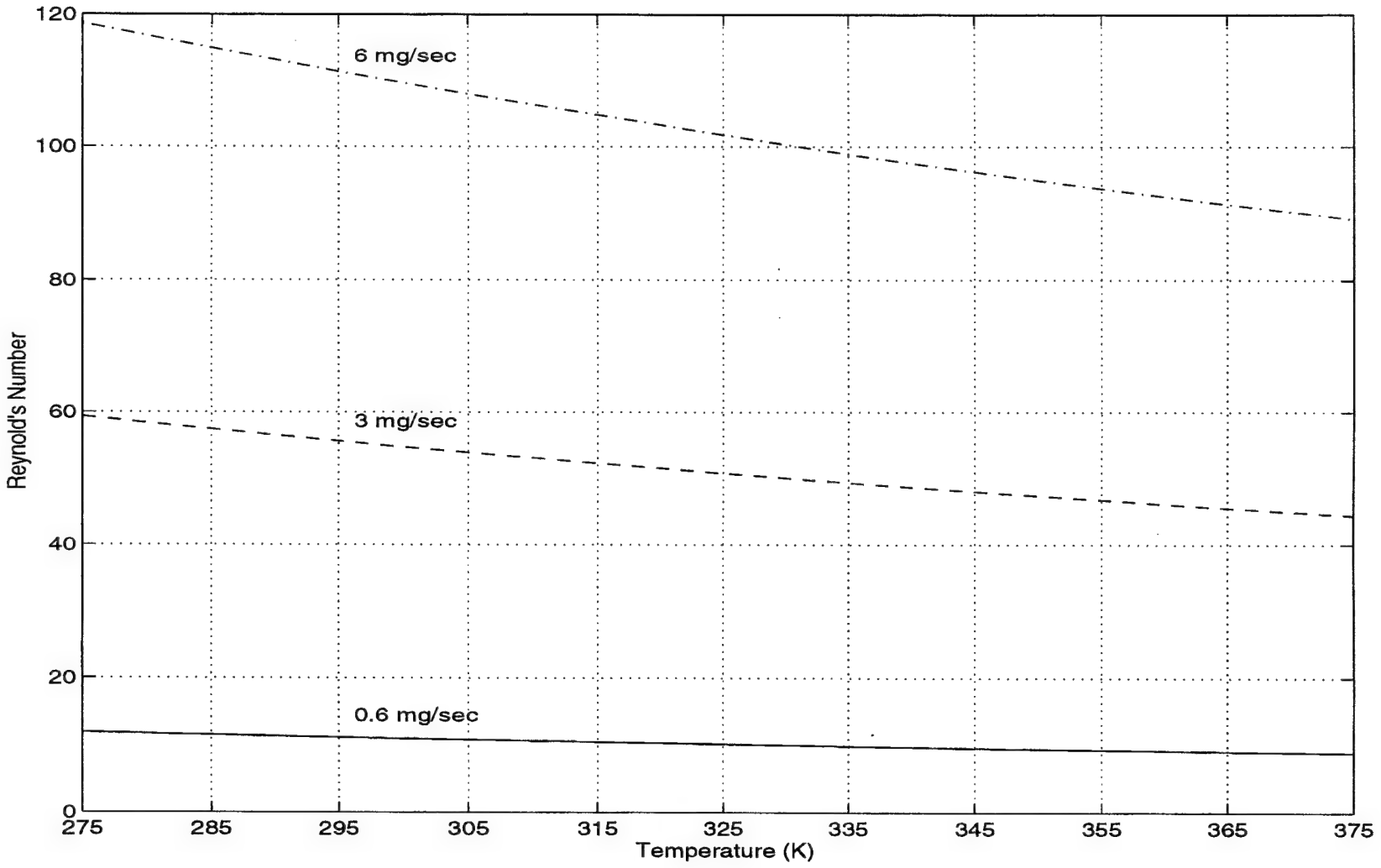

Figure 12. Reynolds number as a function of temperature.

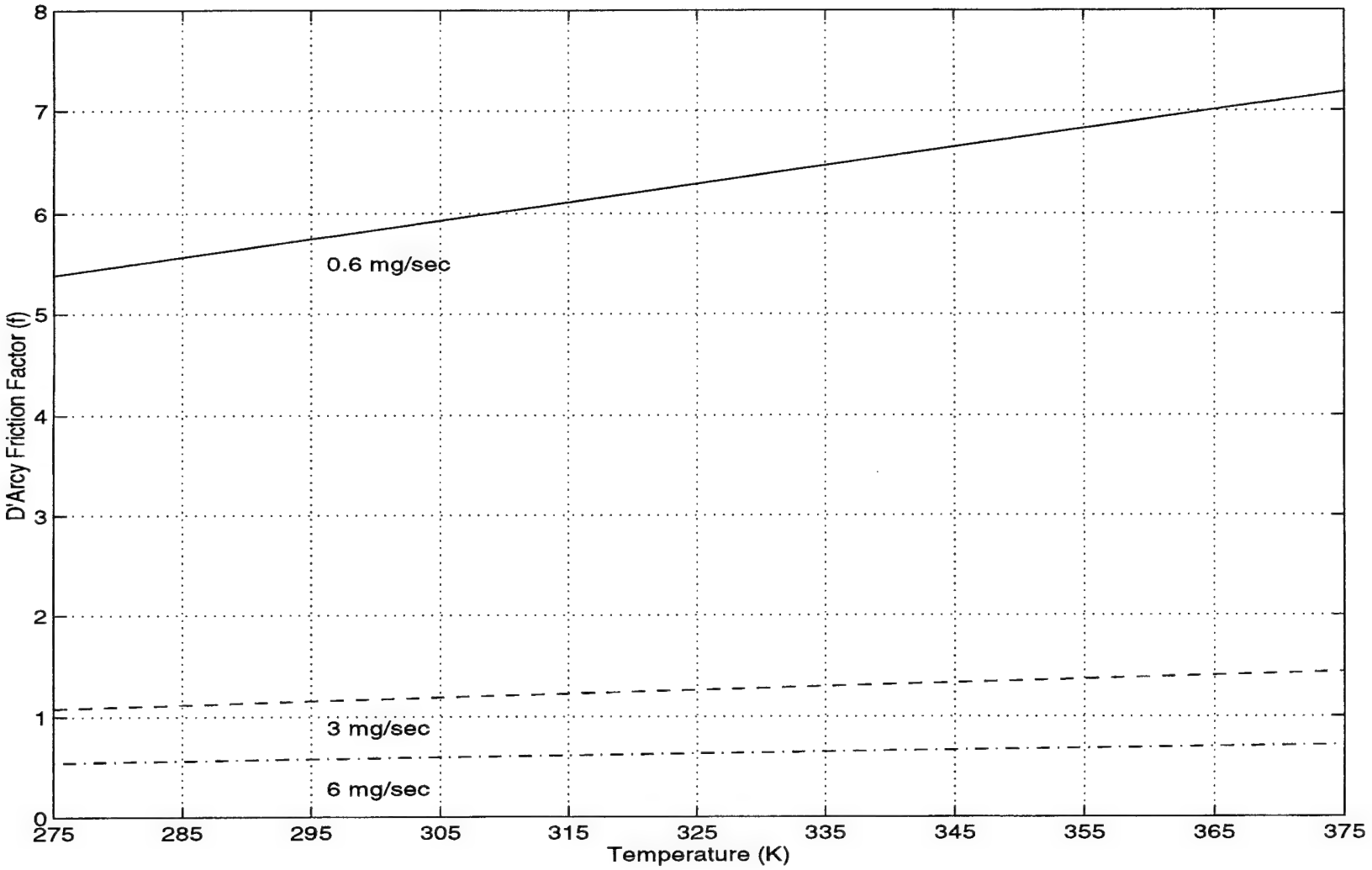

Figure 13. D'Arcy friction factor as a function of temperature.

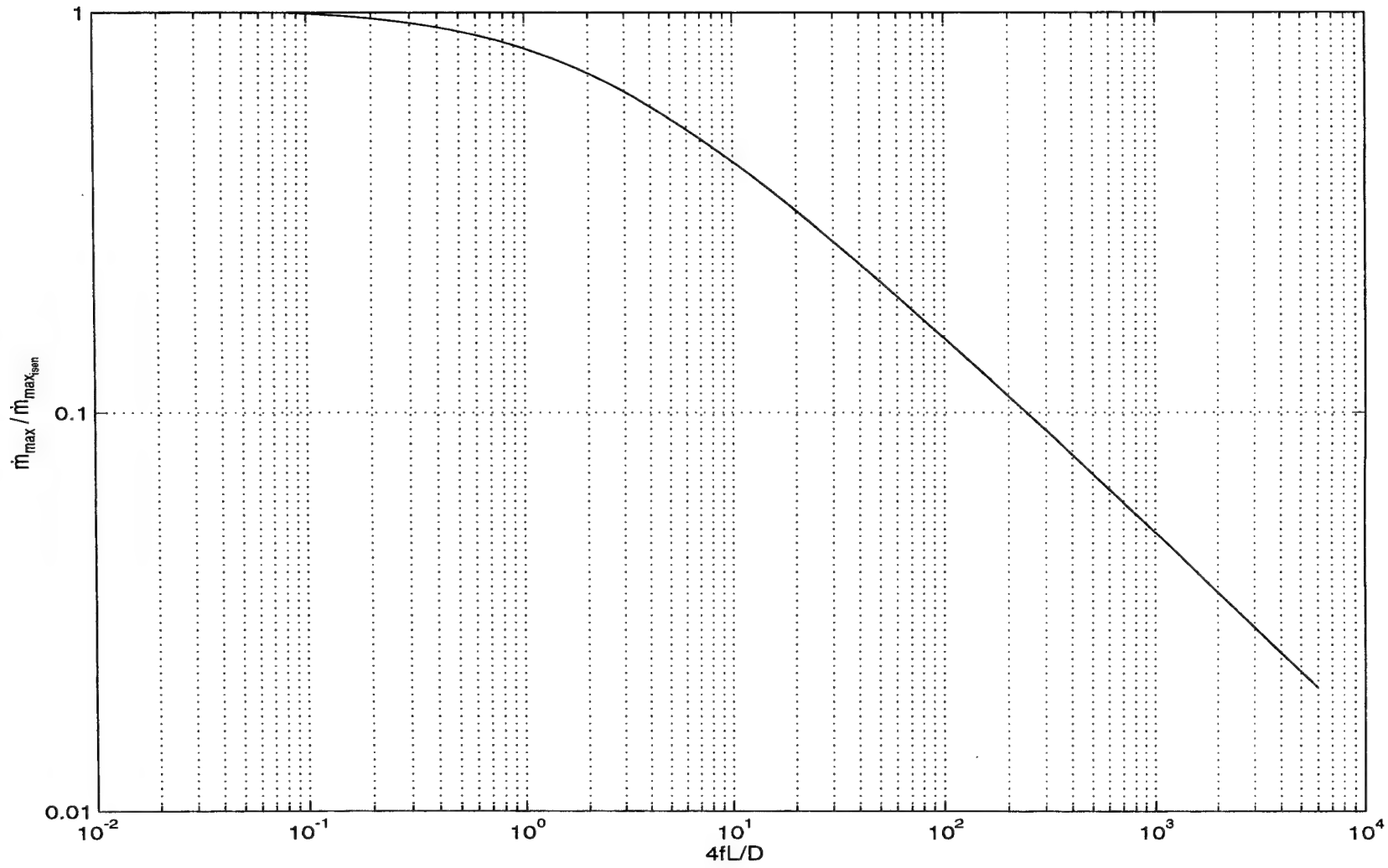

Figure 14. Ratio of choking flow with friction to isentropic choking flow, as a function of $4fL/D$ (γ=1.67).

$4fL/D$. Figure 14 presents such a comparison for γ=1.67. The figure is derived from the fact that, for a choked flow,

$$\dot{m} = \frac{\Gamma P_t^* A^*}{\sqrt{\gamma R T_t^*}} \quad \text{where} \quad \Gamma = \gamma \left[\frac{2}{\gamma + 1} \right]^{\frac{\gamma+1}{2(\gamma-1)}} \tag{4.4}$$

(Note: wherever used in this report, the superscript * refers to the critical, or sonic, condition; the subscript t refers to the stagnation state.) Since, for both Fanno and isentropic flow, the stagnation temperature is constant, the ratio of the Fanno and isentropic flows can be expressed simply as the ratio of the stagnation pressures, which is one of the Fanno flow parameters given in Appendices C and D.

B. BASIC SYSTEM ANALYSIS

It should be apparent from the preceding section that, in the case of a thermal throttling system, mass flow rate and frictional losses are mutually-dependent, a fact which complicates the analysis of such systems. Further, traditional simplified gas dynamics methods, which generally assume some knowledge of conditions at each end of a duct (or a given mass flow rate through it), are insufficient for the analysis of a system in which the fluid undergoes a series of transitions between the points of known conditions, such as is shown in Figure 15. Analysis of these systems is likely to require an iterative process based on some simplifying assumptions. Such a process is presented next.

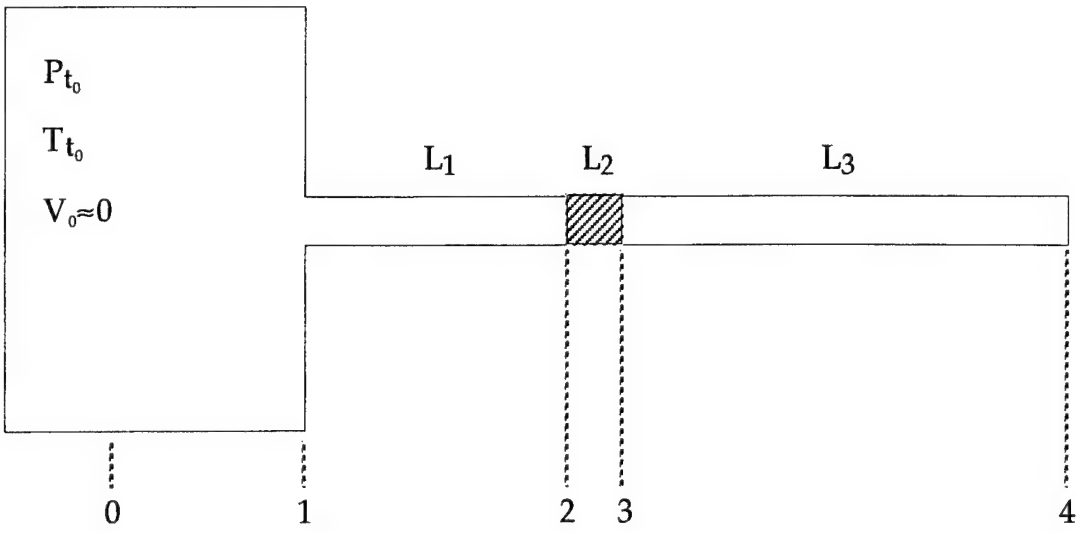

Figure 15. Basic thermothrottle system.

1. General Method

Consider the basic thermothrottle system shown in Figure 15, in which a large tank of xenon at constant pressure and temperature feeds a long constant-area duct with a short thermal throttle between the ends (Stations 2→3). The duct is assumed to be well-insulated, and exhausts to a vacuum. The duct inlet (Station 1) is considered to behave as an isentropic nozzle. The temperature at the outlet of the thermal throttle (Station 3) is known. The flow through the duct is considered to be isothermal Fanno (Appendix D) from Stations 1→2 and 3→4, and Rayleigh (Appendix E) from Stations 2→3.

The general method to be used is to determine the maximum isentropic flow rate through the duct, and to use this flow rate as a means of estimating Mach number and friction coefficient at Station 1. Fanno flow analysis is then used to estimate conditions at Station 2, and Rayleigh flow analysis is used to estimate those at Station 3. The final section of the duct is

considered to be choked at Station 4, and the conditions at Station 3 are used to determine a more accurate friction factor. The problem is then worked back to Station 1 to establish more accurate Mach numbers at each station. These values are used to determine final values for the pressure, density and flow rate at Station 3. The problem can then be reworked for additional combinations of inlet pressure and throttle temperature, or for variations in duct length and/or diameter.

Equations 4.5 through 4.8 allow determination of the maximum isentropic flow rate as a function of tank pressure and temperature.

$$\rho_{t_0} = \frac{P_{t_0}}{RT_{t_0}} \tag{4.5}$$

$$V^* = \sqrt{\frac{2\gamma}{\gamma+1} RT_{t_0}} \tag{4.6}$$

$$\rho^* = \rho_{t_0} \left[\frac{2}{\gamma+1} \right]^{\frac{1}{\gamma-1}} \tag{4.7}$$

$$\dot{m}^*_{isen} = \rho^* A^* V^* \tag{4.8}$$

Once an inlet flow rate has been determined, Equation 4.3 can be used to calculate the friction coefficient in the duct. Equation 4.9 can then be used to determine the Mach number at any station:

$$\frac{4fL^*}{D} = \frac{1-\gamma M^2}{\gamma M^2} + \ln\left(\gamma M^2\right) \tag{4.9}$$

Mach number determination is normally accomplished through the use of tabulated values of the critical length ratio $4fL^*/D$ as a function of inlet Mach number. In this case, however, it is desired to allow the direct calculation of the Mach number for a given value of the critical length ratio. Equation 4.9 cannot be solved explicitly for M, but a series expansion may be employed in place of the logarithmic term (Equation 4.10):

$$\frac{4fL^*}{D}=\frac{1-\gamma M^2}{\gamma M^2}+\left(\gamma M^2-1\right)-\frac{1}{2}\left(\gamma M^2-1\right)^2+\frac{1}{3}\left(\gamma M^2-1\right)^3-\cdots \tag{4.10}$$

The Mach number is considered to be low enough at Stations 1→3 that the higher-order terms in Equation 4.10 can be neglected, resulting in:

$$\frac{4fL^*}{D}=\frac{1-\gamma M^2}{\gamma M^2}+\left(\gamma M^2-1\right)=\left[\frac{1}{\gamma M^2}\right]+\gamma M^2-2 \tag{4.11}$$

It has been determined empirically that the slight modification of Equation 4.12 provides a more accurate curve fit at moderate Mach numbers (below 0.5). Figure 16 shows the correlation between the exact function (Equation 4.9) and the estimate from Equation 4.12. Equation 4.13 gives the desired solution of Equation 4.12 for the Mach number as a function of the critical length ratio:

$$\frac{4fL^*}{D}\cong\left[\frac{0.9}{\gamma M^2}\right]+\gamma M^2-2 \tag{4.12}$$

$$M=\sqrt{\frac{1}{\gamma}\left[1+\frac{y}{2}-\frac{\sqrt{25y^2+100y+10}}{10}\right]}\quad\text{where } y=\frac{4fL}{D} \tag{4.13}$$

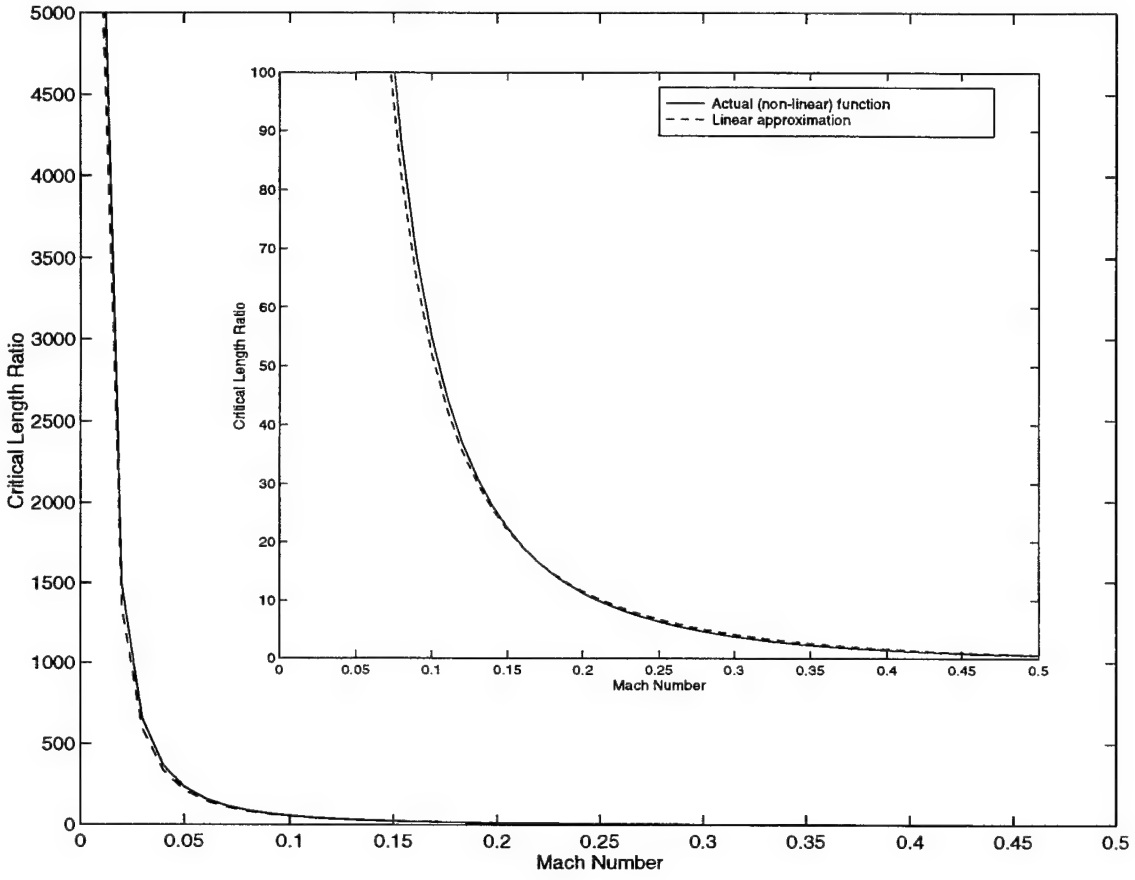

Figure 16. Critical Length Ratio linear approximation.

The Mach number at Station 1 can now be used (in Equations 4.14 through 4.16) to determine the density at Station 1, along with a revised frictional flow rate:

$$\rho_{t_1} = \rho_{t_0}\left[1+\frac{\gamma-1}{2}M_1^2\right]^{\frac{-\gamma}{\gamma-1}} \tag{4.14}$$

$$\rho^{\star} = \rho_{t_1}\sqrt{\gamma}M_1 \tag{4.15}$$

$$\dot{m}^{\star}_{Fanno} = \rho^{\star}A^{\star}V^{\star} \tag{4.16}$$

The solution process is then continued using standard isothermal Fanno flow techniques from Stations 1→2 and Rayleigh flow techniques from Stations 2→3. The result will be revised values for the friction coefficient in both Fanno flow sections, which will then allow for determination of final values for the Mach number at each station, and a final value for the mass flow rate through the duct. Appendix F contains MATLAB code (flowcalc.m) written to automate this process, and to allow for variations in the inlet pressure and in the length and/or diameter of the duct.

2. A Numerical Example

To illustrate the process, consider a system such as the one shown in Figure 15, with initial conditions as given in Table 1 below:

Inlet Temperature	275 K
Inlet Pressure	10 KPa
Throttle Temperature	375 K
L1	0.5 m
L2	0.1 m
L3	0.9 m
Diameter	3 mm

Table 1. Sample system initial conditions.

The MATLAB program flowcalc.m (Appendix F) is used to analyze the system. The code determines a maximum isentropic flow rate of 389 mg/sec, and an unthrottled (275 K throughout the duct) Fanno flow rate of 129 mg/sec, with an initial critical length ratio ($4fL^*/D$) of 16.6. Note that

this value, when used as the input to Figure 14, suggests a flow ratio of about 0.3; the actual calculated ratio is 0.33. The throttled flow rate was calculated to be 5.34 mg/sec, with a critical length ratio of 41 in the first Fanno section and 970 in the second. These values suggest a flow ratio of about (0.25)(0.05)=0.0125; the actual calculated ratio is 0.014. The analysis was then conducted over the entire temperature range of the thermothrottle (275–375 K) for several different pressures. Figure 17 shows a plot of the resulting calculated mass flow rates as a function of temperature.

C. COMPARISON WITH REAL SYSTEMS

There is very little experimental data available on any of the thermal throttling systems currently in use. Most of these systems are based on former-Soviet designs which have been used successfully for many years, but which require very tightly controlled inlet conditions and exhibit very narrow operating ranges. Current ion engine systems using thermal throttles have been designed around these existing throttles. The author is unaware of any case in which a thermal throttle has been operated independently of its engine for the purpose of developing a full set of operating range data—in other words, no one has yet opened up the "black box" to see exactly what is inside. As a result, it is difficult to perform any quantitative comparisons of the predicted flow rates obtained using the methods documented in this report with actual flow rates observed in comparable real-world systems.

The author was given limited access to two Russian ion engine propellant feed system designs, although in neither case was sufficient information available. Significantly, however, the shapes of the flow rate

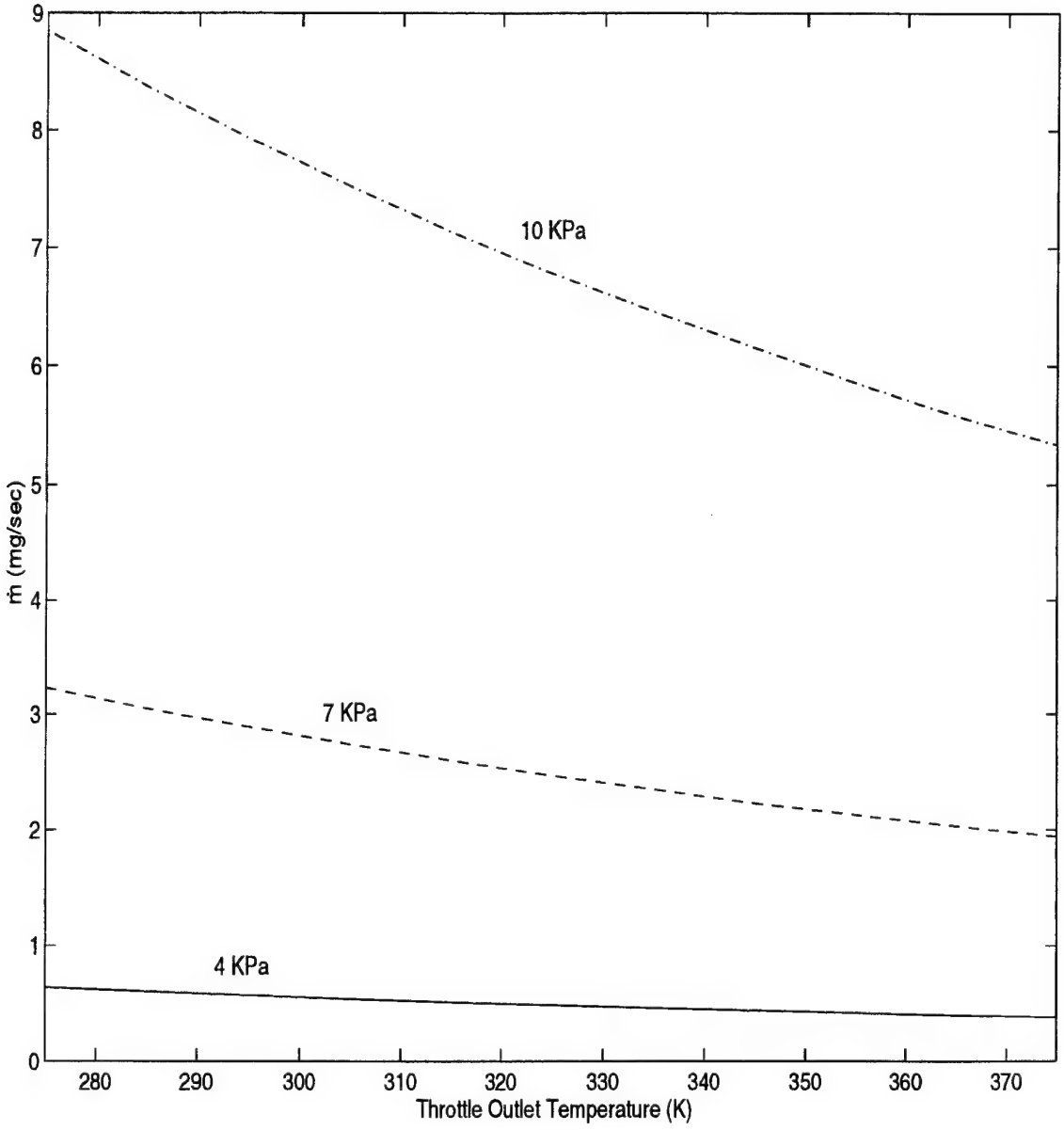

Figure 17. Throttled flow as a function of temperature for several input pressures

curves in Figure 17 are well-supported by the available data, suggesting that the approach used in this report is valid. Other information gained from studying real-world systems is that they are fairly compact (<1 meter from pressure regulator to engine) and that they operate at inlet pressures of 2–3

atmospheres. These systems can be modeled using the MATLAB routine flowcalc.m by varying the input pressure and length parameters, resulting in reasonable agreement with existing systems' measured flow rates.

It should be apparent that the combination of increased inlet pressure and reduced duct length will result in higher flow rates; flowcalc.m can easily verify that fact. Existing systems compensate for their requirements of compactness and higher operating pressures through the use of flow restrictors. There are currently two types of flow restrictors in use in ion engine propellant feed applications. The first, generally referred to as a flow resistor, is shown in Figure 18. Flow resistors are simply sections of duct with reduced areas; they affect flow by increasing the L/D term in the critical length ratio, and can be modeled linearly for laminar flow using a similarity rule developed by Lee (1974).

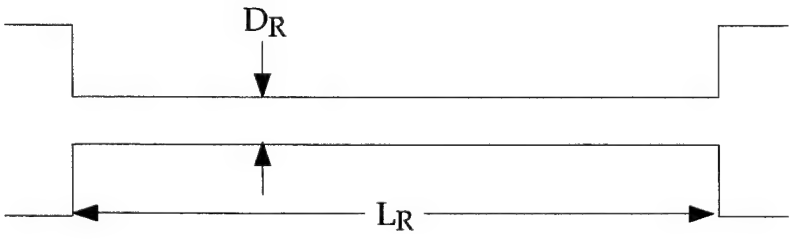

Figure 18. Flow resistor.

The second type of flow restrictor consists of a porous metal plug, occasionally referred to as a sintered restrictor. These are generally designed for a specific combination of gas, input pressure and flow rate. Preliminary work by Martin (1974) using nitrogen gas indicates that, once sufficient data are obtained for a given plug and system combination, it becomes relatively easy to predict the performance of the system under a wider variety of

conditions provided the pressures at the inlet and outlet of the plug are known. That requirement presents a considerable challenge, however, to an analysis based on Fanno and Rayleigh techniques, since a porous plug may be considered as an isenthalpic device which cannot be simply modeled as an equivalent L/D. Figure 19 shows the enthalpy-entropy diagram which may result from the addition of a porous plug at Station 4 in the basic thermothrottle system of Figure 15. Modeling such a system will likely require some knowledge of the temperature and pressure conditions at Station 4, and so will require some degree of instrumentation.

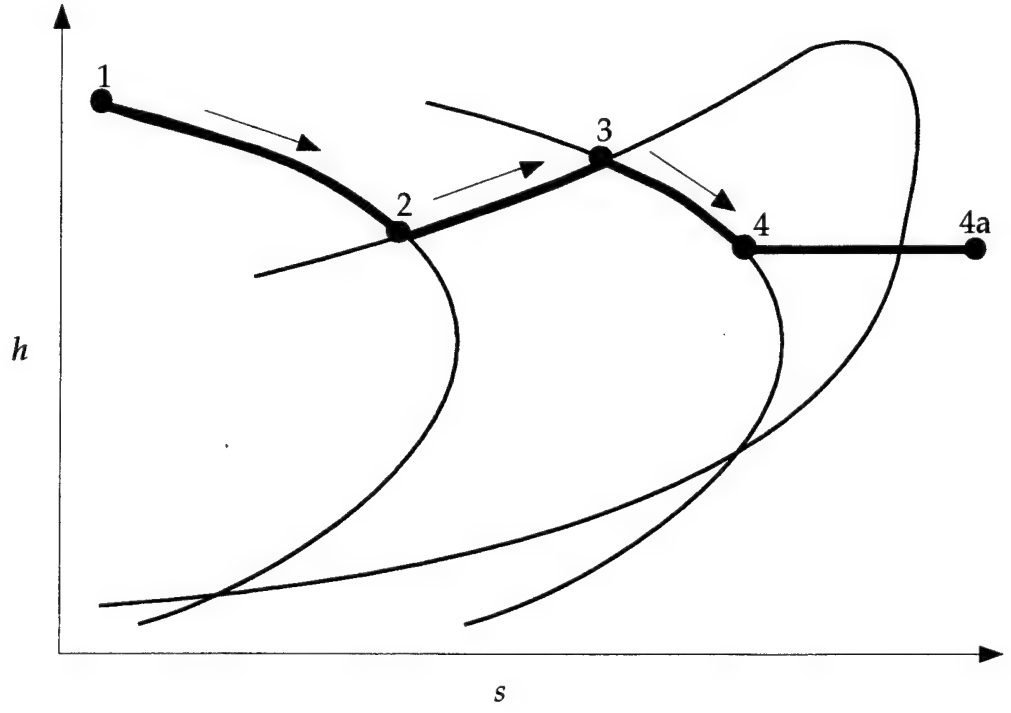

Figure 19. Combined process with isenthalpic flow restrictor.

Another area of interest in the design of current and future thermally-throttled ion engine propulsion systems is the possibility of using the thermal characteristics of the propellant as a substitute for expensive and failure-prone

pressure regulators. Manipulation of the various input parameters in flowcalc.m suggests that a thermothrottle system can be designed to operate over a wider range of input pressures than that used in current systems. However, complete elimination of the need for a pressure regulator would require a system capable of operating under input pressures varying from 1–100 atmospheres. While this could be accomplished using a bank of isolable flow restrictors (which would allow for an extremely large change in L/D over the life of the system), the solenoid valves and tubing connectors required in such a design would add both mass and complexity to the system, and so this likely not an acceptable alternative to the commercially-available pressure regulators currently in use.

Real-world thermal throttling systems generally regulate flow rate as a function of the electrical current supplied to the throttle. This current is used to heat the gas in one of two ways, either through use of an external heating element or by direct current flow through the walls of the throttle; in both cases, heat is produced through I^2R losses. Current flow can be related to gas temperature through a basic heat transfer relationship:

$$q = I^2 R = \left[\frac{Nu_D k}{D}\right](T_w - T_b) \tag{4.17}$$

where Nu_D is the Nusselt number, k is the thermal conductivity of the gas, D is the tubing diameter, and T_w and T_b are the wall and bulk temperatures, respectively. For the uniform heat flux, laminar flow case of a thermal throttle, Nu_D is a constant (4.364), and T_b (which equates to the stagnation temperature of the gas) varies linearly with q (and so with I^2). As a first approximation, it seems that gas flow (which, from Figure 17, varies inversely

with temperature) will, in a lossless system, vary inversely with the square of the current. However, in the uninsulated systems the author has observed, gas flow has tended instead to vary as the inverse of the current.

It will be difficult to predict the exact relationship between throttle current and gas flow rate without knowing which heating method is employed, as well as how effectively the system is insulated, since those factors affect how much of the supplied current is actually used to heat the gas. Also, it must be realized that ground testing is subject to free convection, which depends on the orientation of the heated tubing with respect to gravity; this effect further complicates determination of the current and flow rate relationship. Accordingly, this report has focused on the more well-defined correlation between gas temperature and flow rate.

V. CONCLUSIONS AND RECOMMENDATIONS

A. CONCLUSIONS

This report has presented a possible method for predicting the performance of thermally-throttled ion engine propellant feed systems, based on an adaptation of the traditional gas dynamics approach. While this method appears to agree qualitatively with observed system behavior, it is incomplete in that the means to deal with system components such as porous plugs have not yet been developed.

The results obtained in the previous chapter suggest that a single thermothrottle system, while capable of operating across a wider range of inputs and outputs than is currently seen, is nonetheless unlikely to allow for the complete replacement of the pressure regulators now in use. However, the thermothrottle system does allow for limited variation in input pressure while still delivering the desired flow rates, as opposed to the rigid control of input pressure required in current systems. This flexibility may at least allow for some simplification or reduction in demands on the systems' power processing unit, without much of an additional mass or power requirement.

B. RECOMMENDATIONS

Future study of the thermothrottle concept should focus on an empirical analysis of an operating system as a means of validating or contradicting the approach presented in this report. A simple basic system

such as that depicted in Figure 15 could be easily and inexpensively constructed, and would require only the installation of appropriate instrumentation to assess the accuracy of this report's methods. Such instrumentation should include the means to directly measure gas flow rate, such as through an instrumented orifice or hot wire flow sensor, along with pressure and temperature sensors at the inlet and outlet of the thermothrottle and any system flow restrictors. Given the expense and relative scarcity of xenon gas, argon is suggested as an appropriate substitute, since its characteristics and properties are similar to those of xenon. In the MATLAB program flowcalc.m, for example, only the gas constant R would need to be changed to allow for the analysis of argon in place of xenon.

Alternatively, instrumentation could be installed on one of the thermothrottle systems currently on loan to NASA (which already have the means to measure flow), and direct measurements of the gas temperatures at the throttle inlet and exit, as well as the pressures across any flow restrictors in the system, could be integrated into ongoing ion engine test programs. Since knowledge of the temperature rise across the throttle (along with knowledge and/or control of heat losses in the system) allows determination of the relationship between current and temperature, and knowledge of the pressures at the inlet and exit of flow restrictors allows the remainder of the system to be analyzed according to the Fanno and Rayleigh relationships, these measurements would provide the data necessary to complete the thermothrottle performance prediction model.

APPENDIX A. XENON THERMOPROPERTIES

A. EQUATIONS

1. Specific heat capacity (constant pressure)

$$c_p = 158.416 \frac{\text{J}}{\text{kg} \bullet \text{K}}$$

2. Gas constant

$$R = \frac{\overline{R}}{MW} = 63.323 \frac{\text{J}}{\text{kg} \bullet \text{K}}$$

3. Specific heat capacity (constant volume)

$$c_v = c_p - R = 95.093 \frac{\text{J}}{\text{kg} \bullet \text{K}}$$

4. Specific heat ratio

$$\gamma = \frac{C_p}{C_v} = 1.67$$

5. Enthalpy

$$h = \int c_p dT = c_p T \left[\frac{\text{kJ}}{\text{kg}}\right]$$

6. Internal energy

$$u = h - RT \left[\frac{\text{kJ}}{\text{kg}}\right]$$

7. Entropy function

$$\phi = \int c_p \frac{dT}{T} = c_p \ln T \left[\frac{\text{kJ}}{\text{kg} \bullet \text{K}}\right]$$

8. Acoustic speed

$$a = \sqrt{\gamma RT} \left[\frac{\text{m}}{\text{s}}\right]$$

9. Viscosity

$$\mu = 1.8918 \times 10^{-6} + 6.0506 \times 10^{-8} T + 8.1794 \times 10^{-11} T^2 - 2.0510 \times 10^{-13} T^3 + 2.0165 \times 10^{-16} T^4 - 9.5234 \times 10^{-20} T^5 + 1.7663 \times 10^{-23} T^6 \left[\frac{\text{N} \bullet \text{s}}{\text{m}^2}\right]$$

9. Thermal conductivity

$$k = 1.3554 \times 10^{-6} + 2.0398 \times 10^{-5} T - 5.5381 \times 10^{-9} T^2 \left[\frac{\text{W}}{\text{m} \bullet \text{K}}\right]$$

B. MATLAB CODE

```
% thermoproperties.m
%
% Thermal Properties of Xenon vs. Temperature
%
% Variables (all in SI units):
%
%       T - Temperature
%      CP - Specific Heat at Constant Pressure
%      CV - Specific Heat at Constant Volume
%       g - Gamma (Specific Heat Ratio)
%       R - Gas Constant
%       h - Enthalpy
%       u - Internal Energy
%     PHI - Entropy Function
%      mu - Viscosity
%       k - Thermal Conductivity
%       a - Local Speed of Sound
%
```

```
T1 = [120:10:1000];
T2 = [1050:50:1500];
T = [T1 T2];
T0 = 298.15;

X = ones(size(T));

CP = 158.416*X/1000;

g = 1.67*X;

R = 8.31434/131.29;

CV = CP - R;

h = CP.*(T);

u = h - (R*T);

PHI = CP.*(log(T));

mu = (1E-6)*(1.89178728 + (6.0506328E-2)*T + (8.1793523E-5)*(T.^2) ...
   -(2.051E-7)*(T.^3) + (2.0164963E-10)*(T.^4) - (9.5234E-14)*(T.^5) ...
   +(1.7662669E-17)*(T.^6));

k = 1.355426E-6 + (2.03984913E-5)*T - (5.53807454E-9)*(T.^2);

a = sqrt(g*1000*R.*T);

Y=[T;h;u;PHI;mu;k;a];

fid = fopen('thermoproperties.txt','w');
fprintf(fid,'%2.2f\t %4.4f\t %4.4f\t %4.4f\t %4.4e\t %4.4e\t ...
%4.4f\n',Y);
fclose(fid);
```

Table A.1. Thermodynamic Properties of Xenon in SI Units

T [K]	$h\left[\frac{\text{kJ}}{\text{kg}}\right]$	$u\left[\frac{\text{kJ}}{\text{kg}}\right]$	$\phi\left[\frac{\text{kJ}}{\text{kg}\bullet\text{K}}\right]$	$\mu\left[\frac{\text{N}\bullet\text{s}}{\text{m}^2}\right]$	$k\left[\frac{\text{W}}{\text{m}\bullet\text{K}}\right]$	$a\left[\frac{\text{m}}{\text{s}}\right]$
120.00	19.0099	11.4106	0.7584	1.0015e-05	2.3694e-03	112.6541
130.00	20.5941	12.3614	0.7711	1.0743e-05	2.5596e-03	117.2541
140.00	22.1782	13.3123	0.7828	1.1476e-05	2.7486e-03	121.6803
150.00	23.7624	14.2632	0.7938	1.2211e-05	2.9365e-03	125.9511
160.00	25.3466	15.2141	0.8040	1.2949e-05	3.1233e-03	130.0817
170.00	26.9307	16.1650	0.8136	1.3689e-05	3.3090e-03	134.0852
180.00	28.5149	17.1158	0.8226	1.4431e-05	3.4937e-03	137.9725
190.00	30.0990	18.0667	0.8312	1.5174e-05	3.6771e-03	141.7533
200.00	31.6832	19.0176	0.8393	1.5917e-05	3.8595e-03	145.4358
210.00	33.2674	19.9685	0.8471	1.6661e-05	4.0408e-03	149.0273
220.00	34.8515	20.9193	0.8544	1.7403e-05	4.2210e-03	152.5343
230.00	36.4357	21.8702	0.8615	1.8145e-05	4.4000e-03	155.9625
240.00	38.0198	22.8211	0.8682	1.8886e-05	4.5780e-03	159.3169
250.00	39.6040	23.7720	0.8747	1.9625e-05	4.7548e-03	162.6022
260.00	41.1882	24.7229	0.8809	2.0362e-05	4.9306e-03	165.8223
270.00	42.7723	25.6737	0.8869	2.1096e-05	5.1052e-03	168.9811
280.00	44.3565	26.6246	0.8926	2.1828e-05	5.2787e-03	172.0819
290.00	45.9406	27.5755	0.8982	2.2557e-05	5.4512e-03	175.1279
300.00	47.5248	28.5264	0.9036	2.3282e-05	5.6225e-03	178.1217
310.00	49.1090	29.4773	0.9088	2.4004e-05	5.7927e-03	181.0661
320.00	50.6931	30.4281	0.9138	2.4723e-05	5.9618e-03	183.9633
330.00	52.2773	31.3790	0.9187	2.5437e-05	6.1298e-03	186.8157
340.00	53.8614	32.3299	0.9234	2.6147e-05	6.2966e-03	189.6251
350.00	55.4456	33.2808	0.9280	2.6853e-05	6.4624e-03	192.3935
360.00	57.0298	34.2317	0.9325	2.7555e-05	6.6271e-03	195.1226
370.00	58.6139	35.1825	0.9368	2.8252e-05	6.7906e-03	197.8141
380.00	60.1981	36.1334	0.9410	2.8944e-05	6.9531e-03	200.4694
390.00	61.7822	37.0843	0.9451	2.9632e-05	7.1144e-03	203.0900
400.00	63.3664	38.0352	0.9491	3.0314e-05	7.2747e-03	205.6773
410.00	64.9506	38.9861	0.9531	3.0992e-05	7.4338e-03	208.2324
420.00	66.5347	39.9369	0.9569	3.1664e-05	7.5918e-03	210.7565
430.00	68.1189	40.8878	0.9606	3.2332e-05	7.7487e-03	213.2507
440.00	69.7030	41.8387	0.9642	3.2994e-05	7.9045e-03	215.7161
450.00	71.2872	42.7896	0.9678	3.3651e-05	8.0592e-03	218.1537
460.00	72.8714	43.7405	0.9713	3.4303e-05	8.2128e-03	220.5643
470.00	74.4555	44.6913	0.9747	3.4950e-05	8.3653e-03	222.9488
480.00	76.0397	45.6422	0.9780	3.5591e-05	8.5167e-03	225.3082
490.00	77.6238	46.5931	0.9813	3.6228e-05	8.6669e-03	227.6430
500.00	79.2080	47.5440	0.9845	3.6859e-05	8.8161e-03	229.9542
510.00	80.7922	48.4949	0.9876	3.7485e-05	8.9641e-03	232.2423
520.00	82.3763	49.4457	0.9907	3.8106e-05	9.1111e-03	234.5082
530.00	83.9605	50.3966	0.9937	3.8721e-05	9.2569e-03	236.7523
540.00	85.5446	51.3475	0.9967	3.9332e-05	9.4016e-03	238.9754
550.00	87.1288	52.2984	0.9996	3.9937e-05	9.5453e-03	241.1780
560.00	88.7130	53.2493	1.0024	4.0538e-05	9.6878e-03	243.3606
570.00	90.2971	54.2001	1.0053	4.1134e-05	9.8292e-03	245.5239
580.00	91.8813	55.1510	1.0080	4.1725e-05	9.9695e-03	247.6682
590.00	93.4654	56.1019	1.0107	4.2311e-05	1.0109e-02	249.7942
600.00	95.0496	57.0528	1.0134	4.2892e-05	1.0247e-02	251.9022
610.00	96.6338	58.0036	1.0160	4.3469e-05	1.0384e-02	253.9927
620.00	98.2179	58.9545	1.0186	4.4041e-05	1.0520e-02	256.0661

Table A.1. Thermodynamic Properties of Xenon in SI Units (cont.)

T [K]	$h\left[\frac{\text{kJ}}{\text{kg}}\right]$	$u\left[\frac{\text{kJ}}{\text{kg}}\right]$	$\phi\left[\frac{\text{kJ}}{\text{kg}\bullet\text{K}}\right]$	$\mu\left[\frac{\text{N}\bullet\text{s}}{\text{m}^2}\right]$	$k\left[\frac{\text{W}}{\text{m}\bullet\text{K}}\right]$	$a\left[\frac{\text{m}}{\text{s}}\right]$
630.00	99.8021	59.9054	1.0211	4.4609e-05	1.0654e-02	258.1229
640.00	101.3862	60.8563	1.0236	4.5172e-05	1.0788e-02	260.1635
650.00	102.9704	61.8072	1.0261	4.5731e-05	1.0921e-02	262.1881
660.00	104.5546	62.7580	1.0285	4.6286e-05	1.1052e-02	264.1972
670.00	106.1387	63.7089	1.0309	4.6836e-05	1.1182e-02	266.1912
680.00	107.7229	64.6598	1.0332	4.7383e-05	1.1312e-02	268.1703
690.00	109.3070	65.6107	1.0355	4.7925e-05	1.1440e-02	270.1350
700.00	110.8912	66.5616	1.0378	4.8464e-05	1.1567e-02	272.0855
710.00	112.4754	67.5124	1.0400	4.8999e-05	1.1693e-02	274.0220
720.00	114.0595	68.4633	1.0423	4.9530e-05	1.1817e-02	275.9450
730.00	115.6437	69.4142	1.0444	5.0057e-05	1.1941e-02	277.8547
740.00	117.2278	70.3651	1.0466	5.0581e-05	1.2064e-02	279.7513
750.00	118.8120	71.3160	1.0487	5.1101e-05	1.2185e-02	281.6352
760.00	120.3962	72.2668	1.0508	5.1618e-05	1.2305e-02	283.5066
770.00	121.9803	73.2177	1.0529	5.2132e-05	1.2425e-02	285.3656
780.00	123.5645	74.1686	1.0549	5.2642e-05	1.2543e-02	287.2127
790.00	125.1486	75.1195	1.0570	5.3149e-05	1.2660e-02	289.0479
800.00	126.7328	76.0704	1.0589	5.3653e-05	1.2776e-02	290.8716
810.00	128.3170	77.0212	1.0609	5.4154e-05	1.2891e-02	292.6839
820.00	129.9011	77.9721	1.0629	5.4652e-05	1.3004e-02	294.4850
830.00	131.4853	78.9230	1.0648	5.5147e-05	1.3117e-02	296.2752
840.00	133.0694	79.8739	1.0667	5.5639e-05	1.3228e-02	298.0547
850.00	134.6536	80.8248	1.0686	5.6129e-05	1.3339e-02	299.8236
860.00	136.2378	81.7756	1.0704	5.6616e-05	1.3448e-02	301.5821
870.00	137.8219	82.7265	1.0722	5.7100e-05	1.3556e-02	303.3304
880.00	139.4061	83.6774	1.0740	5.7581e-05	1.3663e-02	305.0687
890.00	140.9902	84.6283	1.0758	5.8060e-05	1.3769e-02	306.7971
900.00	142.5744	85.5792	1.0776	5.8537e-05	1.3874e-02	308.5159
910.00	144.1586	86.5300	1.0794	5.9011e-05	1.3978e-02	310.2251
920.00	145.7427	87.4809	1.0811	5.9482e-05	1.4081e-02	311.9250
930.00	147.3269	88.4318	1.0828	5.9951e-05	1.4182e-02	313.6157
940.00	148.9110	89.3827	1.0845	6.0418e-05	1.4282e-02	315.2973
950.00	150.4952	90.3336	1.0862	6.0882e-05	1.4382e-02	316.9700
960.00	152.0794	91.2844	1.0878	6.1344e-05	1.4480e-02	318.6339
970.00	153.6635	92.2353	1.0895	6.1804e-05	1.4577e-02	320.2891
980.00	155.2477	93.1862	1.0911	6.2262e-05	1.4673e-02	321.9358
990.00	156.8318	94.1371	1.0927	6.2717e-05	1.4768e-02	323.5742
1000.00	158.4160	95.0879	1.0943	6.3170e-05	1.4862e-02	325.2043
1050.00	166.3368	99.8423	1.1020	6.5403e-05	1.5314e-02	333.2353
1100.00	174.2576	104.5967	1.1094	6.7581e-05	1.5739e-02	341.0772
1150.00	182.1784	109.3511	1.1164	6.9706e-05	1.6136e-02	348.7428
1200.00	190.0992	114.1055	1.1232	7.1778e-05	1.6505e-02	356.2435
1250.00	198.0200	118.8599	1.1296	7.3796e-05	1.6846e-02	363.5895
1300.00	205.9408	123.6143	1.1359	7.5765e-05	1.7160e-02	370.7900
1350.00	213.8616	128.3687	1.1418	7.7689e-05	1.7446e-02	377.8533
1400.00	221.7824	133.1231	1.1476	7.9579e-05	1.7705e-02	384.7869
1450.00	229.7032	137.8775	1.1532	8.1452e-05	1.7935e-02	391.5979
1500.00	237.6240	142.6319	1.1585	8.3331e-05	1.8138e-02	398.2923

APPENDIX B. ISENTROPIC FLOW PROPERTIES

A. EQUATIONS

1. Dimensionless velocity

$$M^* = \sqrt{\frac{(\gamma+1)M^2}{2+(\gamma-1)M^2}}$$

2. Temperature ratio

$$\frac{T}{T_t} = \left[1+\frac{\gamma-1}{2}M^2\right]^{-1}$$

3. Pressure ratio

$$\frac{P}{P_t} = \left[1+\frac{\gamma-1}{2}M^2\right]^{\frac{-\gamma}{\gamma-1}}$$

4. Density ratio

$$\frac{\rho}{\rho_t} = \left[1+\frac{\gamma-1}{2}M^2\right]^{\frac{-1}{\gamma-1}}$$

5. Area ratio

$$\frac{A}{A^*} = \frac{1}{M}\left\{\frac{2}{\gamma+1}\left[1+\frac{\gamma-1}{2}M^2\right]\right\}^{\frac{\gamma+1}{2(\gamma-1)}}$$

B. MATLAB CODE

```
% Isentropic.m
%
% Isentropic flow parameters
%
% Variables:
%
%           M - Mach Number
%           k - Gamma (Specific Heat Ratio)
%       MSTAR - Dimensionless Velocity
%        TRAT - Stagnation Temperature Ratio
%        PRAT - Stagnation Pressure Ratio
%     RHOTRAT - Stagnation Density Ratio
%        ARAT - Critical Area Ratio
%
M = [0:.01:1];

k = 1.67;

MSTAR = sqrt(((k+1).*M.^2)./(2+(k-1).*M.^2));

TRAT = 1./(1+((k-1)/2).*M.^2);

PRAT = (1+((k-1)/2).*M.^2).^(-k/(k-1));

RHORAT = (1+((k-1)/2).*M.^2).^(-1/(k-1));

ARAT = (1./M).*((2/(k+1)).*(1+((k-1)/2).*M.^2)).^((k+1)/(2*(k-1)));

Y=[M;MSTAR;TRAT;PRAT;RHORAT;ARAT];

fid = fopen('isentropic.txt','w');
fprintf(fid,'%2.2f\t %4.4e\t %4.4e\t %4.4e\t %4.4e\t %4.4e\n',Y);
fclose(fid);
```

Table B.1. Isentropic Flow (γ=1.67)

M	M^*	$\frac{T}{T_t}$	$\frac{P}{P_t}$	$\frac{\rho}{\rho_t}$	$\frac{A}{A^*}$
0.00	0.0000e+00	1.0000e+00	1.0000e+00	1.0000e+00	∞
0.01	1.1554e-02	9.9997e-01	9.9992e-01	9.9995e-01	5.6235e+01
0.02	2.3107e-02	9.9987e-01	9.9967e-01	9.9980e-01	2.8123e+01
0.03	3.4657e-02	9.9970e-01	9.9925e-01	9.9955e-01	1.8755e+01
0.04	4.6204e-02	9.9946e-01	9.9867e-01	9.9920e-01	1.4073e+01
0.05	5.7747e-02	9.9916e-01	9.9792e-01	9.9875e-01	1.1265e+01
0.06	6.9284e-02	9.9880e-01	9.9700e-01	9.9820e-01	9.3943e+00
0.07	8.0813e-02	9.9836e-01	9.9592e-01	9.9756e-01	8.0593e+00
0.08	9.2335e-02	9.9786e-01	9.9468e-01	9.9681e-01	7.0589e+00
0.09	1.0385e-01	9.9729e-01	9.9327e-01	9.9596e-01	6.2817e+00
0.10	1.1535e-01	9.9666e-01	9.9170e-01	9.9502e-01	5.6607e+00
0.11	1.2684e-01	9.9596e-01	9.8997e-01	9.9398e-01	5.1533e+00
0.12	1.3832e-01	9.9520e-01	9.8808e-01	9.9284e-01	4.7310e+00
0.13	1.4978e-01	9.9437e-01	9.8603e-01	9.9161e-01	4.3744e+00
0.14	1.6123e-01	9.9348e-01	9.8382e-01	9.9028e-01	4.0692e+00
0.15	1.7266e-01	9.9252e-01	9.8146e-01	9.8885e-01	3.8052e+00
0.16	1.8408e-01	9.9150e-01	9.7894e-01	9.8734e-01	3.5747e+00
0.17	1.9548e-01	9.9041e-01	9.7627e-01	9.8572e-01	3.3718e+00
0.18	2.0686e-01	9.8926e-01	9.7345e-01	9.8402e-01	3.1919e+00
0.19	2.1821e-01	9.8805e-01	9.7048e-01	9.8222e-01	3.0313e+00
0.20	2.2955e-01	9.8678e-01	9.6737e-01	9.8033e-01	2.8871e+00
0.21	2.4087e-01	9.8544e-01	9.6411e-01	9.7835e-01	2.7571e+00
0.22	2.5216e-01	9.8404e-01	9.6070e-01	9.7628e-01	2.6392e+00
0.23	2.6342e-01	9.8259e-01	9.5716e-01	9.7412e-01	2.5319e+00
0.24	2.7466e-01	9.8107e-01	9.5348e-01	9.7188e-01	2.4339e+00
0.25	2.8588e-01	9.7949e-01	9.4966e-01	9.6955e-01	2.3440e+00
0.26	2.9706e-01	9.7786e-01	9.4571e-01	9.6713e-01	2.2614e+00
0.27	3.0822e-01	9.7616e-01	9.4163e-01	9.6463e-01	2.1852e+00
0.28	3.1935e-01	9.7441e-01	9.3742e-01	9.6204e-01	2.1147e+00
0.29	3.3045e-01	9.7260e-01	9.3309e-01	9.5938e-01	2.0494e+00
0.30	3.4152e-01	9.7073e-01	9.2864e-01	9.5663e-01	1.9886e+00
0.31	3.5255e-01	9.6881e-01	9.2406e-01	9.5381e-01	1.9321e+00
0.32	3.6355e-01	9.6683e-01	9.1937e-01	9.5090e-01	1.8794e+00
0.33	3.7452e-01	9.6480e-01	9.1456e-01	9.4792e-01	1.8301e+00
0.34	3.8545e-01	9.6272e-01	9.0964e-01	9.4487e-01	1.7839e+00
0.35	3.9635e-01	9.6058e-01	9.0462e-01	9.4174e-01	1.7406e+00
0.36	4.0721e-01	9.5839e-01	8.9949e-01	9.3854e-01	1.7000e+00
0.37	4.1803e-01	9.5615e-01	8.9425e-01	9.3526e-01	1.6618e+00
0.38	4.2881e-01	9.5386e-01	8.8892e-01	9.3192e-01	1.6258e+00
0.39	4.3956e-01	9.5152e-01	8.8349e-01	9.2851e-01	1.5919e+00
0.40	4.5026e-01	9.4913e-01	8.7797e-01	9.2503e-01	1.5599e+00
0.41	4.6092e-01	9.4669e-01	8.7236e-01	9.2149e-01	1.5297e+00
0.42	4.7154e-01	9.4420e-01	8.6666e-01	9.1788e-01	1.5011e+00
0.43	4.8212e-01	9.4167e-01	8.6088e-01	9.1421e-01	1.4740e+00
0.44	4.9266e-01	9.3909e-01	8.5502e-01	9.1047e-01	1.4484e+00
0.45	5.0315e-01	9.3647e-01	8.4908e-01	9.0668e-01	1.4242e+00
0.46	5.1360e-01	9.3381e-01	8.4307e-01	9.0283e-01	1.4011e+00
0.47	5.2401e-01	9.3110e-01	8.3699e-01	8.9893e-01	1.3793e+00
0.48	5.3436e-01	9.2835e-01	8.3084e-01	8.9497e-01	1.3585e+00
0.49	5.4468e-01	9.2555e-01	8.2462e-01	8.9095e-01	1.3388e+00
0.50	5.5494e-01	9.2272e-01	8.1835e-01	8.8688e-01	1.3201e+00

Table B.1. Isentropic Flow (γ=1.67) (cont.)

M	M^*	$\frac{T}{T_t}$	$\frac{P}{P_t}$	$\frac{\rho}{\rho_t}$	$\frac{A}{A^*}$
0.51	5.6516e-01	9.1985e-01	8.1201e-01	8.8277e-01	1.3023e+00
0.52	5.7533e-01	9.1694e-01	8.0563e-01	8.7860e-01	1.2853e+00
0.53	5.8545e-01	9.1399e-01	7.9919e-01	8.7439e-01	1.2692e+00
0.54	5.9552e-01	9.1101e-01	7.9270e-01	8.7013e-01	1.2538e+00
0.55	6.0554e-01	9.0799e-01	7.8616e-01	8.6583e-01	1.2392e+00
0.56	6.1551e-01	9.0493e-01	7.7958e-01	8.6148e-01	1.2253e+00
0.57	6.2543e-01	9.0184e-01	7.7297e-01	8.5710e-01	1.2120e+00
0.58	6.3530e-01	8.9872e-01	7.6631e-01	8.5267e-01	1.1994e+00
0.59	6.4512e-01	8.9557e-01	7.5963e-01	8.4821e-01	1.1873e+00
0.60	6.5489e-01	8.9238e-01	7.5291e-01	8.4371e-01	1.1759e+00
0.61	6.6460e-01	8.8916e-01	7.4616e-01	8.3918e-01	1.1649e+00
0.62	6.7426e-01	8.8592e-01	7.3939e-01	8.3461e-01	1.1545e+00
0.63	6.8387e-01	8.8264e-01	7.3260e-01	8.3001e-01	1.1446e+00
0.64	6.9342e-01	8.7934e-01	7.2579e-01	8.2538e-01	1.1352e+00
0.65	7.0292e-01	8.7601e-01	7.1896e-01	8.2072e-01	1.1262e+00
0.66	7.1237e-01	8.7266e-01	7.1211e-01	8.1603e-01	1.1176e+00
0.67	7.2176e-01	8.6928e-01	7.0526e-01	8.1132e-01	1.1095e+00
0.68	7.3110e-01	8.6587e-01	6.9840e-01	8.0658e-01	1.1018e+00
0.69	7.4038e-01	8.6245e-01	6.9153e-01	8.0182e-01	1.0944e+00
0.70	7.4961e-01	8.5900e-01	6.8465e-01	7.9704e-01	1.0874e+00
0.71	7.5878e-01	8.5552e-01	6.7778e-01	7.9224e-01	1.0808e+00
0.72	7.6789e-01	8.5203e-01	6.7090e-01	7.8741e-01	1.0745e+00
0.73	7.7695e-01	8.4852e-01	6.6403e-01	7.8258e-01	1.0685e+00
0.74	7.8596e-01	8.4499e-01	6.5717e-01	7.7772e-01	1.0629e+00
0.75	7.9490e-01	8.4144e-01	6.5031e-01	7.7285e-01	1.0576e+00
0.76	8.0379e-01	8.3787e-01	6.4346e-01	7.6797e-01	1.0525e+00
0.77	8.1263e-01	8.3429e-01	6.3662e-01	7.6307e-01	1.0478e+00
0.78	8.2140e-01	8.3069e-01	6.2980e-01	7.5816e-01	1.0433e+00
0.79	8.3012e-01	8.2708e-01	6.2299e-01	7.5325e-01	1.0391e+00
0.80	8.3878e-01	8.2345e-01	6.1620e-01	7.4832e-01	1.0351e+00
0.81	8.4739e-01	8.1981e-01	6.0944e-01	7.4339e-01	1.0314e+00
0.82	8.5594e-01	8.1616e-01	6.0269e-01	7.3845e-01	1.0279e+00
0.83	8.6443e-01	8.1249e-01	5.9596e-01	7.3350e-01	1.0247e+00
0.84	8.7286e-01	8.0882e-01	5.8927e-01	7.2855e-01	1.0217e+00
0.85	8.8124e-01	8.0513e-01	5.8259e-01	7.2360e-01	1.0189e+00
0.86	8.8955e-01	8.0143e-01	5.7595e-01	7.1865e-01	1.0163e+00
0.87	8.9782e-01	7.9773e-01	5.6934e-01	7.1370e-01	1.0139e+00
0.88	9.0602e-01	7.9401e-01	5.6275e-01	7.0874e-01	1.0118e+00
0.89	9.1417e-01	7.9029e-01	5.5620e-01	7.0379e-01	1.0098e+00
0.90	9.2225e-01	7.8657e-01	5.4969e-01	6.9884e-01	1.0081e+00
0.91	9.3029e-01	7.8283e-01	5.4321e-01	6.9390e-01	1.0065e+00
0.92	9.3826e-01	7.7909e-01	5.3676e-01	6.8896e-01	1.0051e+00
0.93	9.4618e-01	7.7535e-01	5.3036e-01	6.8402e-01	1.0039e+00
0.94	9.5404e-01	7.7160e-01	5.2399e-01	6.7909e-01	1.0028e+00
0.95	9.6184e-01	7.6785e-01	5.1766e-01	6.7417e-01	1.0019e+00
0.96	9.6958e-01	7.6410e-01	5.1138e-01	6.6926e-01	1.0012e+00
0.97	9.7727e-01	7.6034e-01	5.0513e-01	6.6435e-01	1.0007e+00
0.98	9.8491e-01	7.5658e-01	4.9893e-01	6.5946e-01	1.0003e+00
0.99	9.9248e-01	7.5282e-01	4.9278e-01	6.5458e-01	1.0001e+00
1.00	1.0000e+00	7.4906e-01	4.8667e-01	6.4970e-01	1.0000e+00

APPENDIX C. FANNO FLOW PROPERTIES

A. EQUATIONS

1. Dimensionless velocity

$$M^{\star}=\frac{\rho^{\star}}{\rho}=M\left\{\left[\frac{2}{\gamma+1}\right]\left[1+\frac{\gamma-1}{2}M^{2}\right]\right\}^{-\frac{1}{2}}$$

2. Critical temperature ratio

$$\frac{T}{T^{\star}}=\left\{\left[\frac{2}{\gamma+1}\right]\left[1+\frac{\gamma-1}{2}M^{2}\right]\right\}^{-1}$$

3. Critical pressure ratio

$$\frac{P}{P^{\star}}=\frac{1}{M}\left\{\left[\frac{2}{\gamma+1}\right]\left[1+\frac{\gamma-1}{2}M^{2}\right]\right\}^{-\frac{1}{2}}$$

4. Critical stagnation pressure ratio

$$\frac{P_{t}}{P_{t}^{\star}}=\frac{1}{M}\left\{\left[\frac{2}{\gamma+1}\right]\left[1+\frac{\gamma-1}{2}M^{2}\right]\right\}^{\frac{\gamma+1}{2(\gamma-1)}}$$

5. Critical length ratio

$$\frac{4fL^{\star}}{D}=\frac{1-M^{2}}{\gamma M^{2}}+\left[\frac{\gamma+1}{2\gamma}\right]\ln\left[M^{2}\left\{\left[\frac{2}{\gamma+1}\right]\left[1+\frac{\gamma-1}{2}M^{2}\right]\right\}^{-1}\right]$$

B. MATLAB CODE

```
% Fanno.m
%
% Fanno flow parameters
%
% Variables:
%
%           M - Mach Number
%           k - Gamma (Specific Heat Ratio)
%       MSTAR - Dimensionless Velocity
%        TRAT - Static Temperature Ratio
%        PRAT - Static Pressure Ratio
%     BIGPRAT - Stagnation Pressure Ratio
%      FLDRAT - Critical Length Ratio
%
M = [0:.01:1];

k = 1.67;

MSTAR = M.*(((2/(k+1))*(1+(((k-1)/2).*M.^2))).^(-.5));

TRAT = ((2/(k+1))*(1+(((k-1)/2).*M.^2))).^(-1);

PRAT = (1./M).*(((2/(k+1))*(1+(((k-1)/2).*M.^2))).^(-.5));

BIGPRAT = (1./M).*(((2/(k+1))*(1+(((k-1)/2).*M.^2))).^((k+1)/(2* ...
          (k-1))));

FLDRAT = ((1-M.^2)./(k.*(M.^2)))+((k+1)/(2*k)).*log((M.^2).*(TRAT));

Y=[M;MSTAR;TRAT;PRAT;BIGPRAT;FLDRAT];

fid = fopen('fanno.txt','w');
fprintf(fid,'%2.2f\t %4.4e\t %4.4e\t %4.4e\t %4.4e\n',Y);
fclose(fid);
```

Table C.1. Fanno Flow (γ=1.67)

M	$M^* = \frac{\rho^*}{\rho}$	$\frac{T}{T^*}$	$\frac{P}{P^*}$	$\frac{P_t}{P_t^*}$	$\frac{4fL^*}{D}$
0.00	0.0000e+00	1.3350e+00	∞	∞	∞
0.01	1.1554e-02	1.3350e+00	1.1554e+02	5.6235e+01	5.9803e+03
0.02	2.3107e-02	1.3348e+00	5.7767e+01	2.8123e+01	1.4904e+03
0.03	3.4657e-02	1.3346e+00	3.8508e+01	1.8755e+01	6.5936e+02
0.04	4.6204e-02	1.3343e+00	2.8878e+01	1.4073e+01	3.6874e+02
0.05	5.7747e-02	1.3339e+00	2.3099e+01	1.1265e+01	2.3436e+02
0.06	6.9284e-02	1.3334e+00	1.9245e+01	9.3943e+00	1.6147e+02
0.07	8.0813e-02	1.3328e+00	1.6492e+01	8.0593e+00	1.1758e+02
0.08	9.2335e-02	1.3321e+00	1.4427e+01	7.0589e+00	8.9155e+01
0.09	1.0385e-01	1.3314e+00	1.2821e+01	6.2817e+00	6.9706e+01
0.10	1.1535e-01	1.3305e+00	1.1535e+01	5.6607e+00	5.5828e+01
0.11	1.2684e-01	1.3296e+00	1.0483e+01	5.1533e+00	4.5588e+01
0.12	1.3832e-01	1.3286e+00	9.6054e+00	4.7310e+00	3.7822e+01
0.13	1.4978e-01	1.3275e+00	8.8628e+00	4.3744e+00	3.1798e+01
0.14	1.6123e-01	1.3263e+00	8.2261e+00	4.0692e+00	2.7035e+01
0.15	1.7266e-01	1.3250e+00	7.6739e+00	3.8052e+00	2.3206e+01
0.16	1.8408e-01	1.3236e+00	7.1906e+00	3.5747e+00	2.0086e+01
0.17	1.9548e-01	1.3222e+00	6.7639e+00	3.3718e+00	1.7511e+01
0.18	2.0686e-01	1.3207e+00	6.3845e+00	3.1919e+00	1.5363e+01
0.19	2.1821e-01	1.3190e+00	6.0447e+00	3.0313e+00	1.3555e+01
0.20	2.2955e-01	1.3173e+00	5.7388e+00	2.8871e+00	1.2018e+01
0.21	2.4087e-01	1.3156e+00	5.4618e+00	2.7571e+00	1.0704e+01
0.22	2.5216e-01	1.3137e+00	5.2099e+00	2.6392e+00	9.5705e+00
0.23	2.6342e-01	1.3118e+00	4.9796e+00	2.5319e+00	8.5879e+00
0.24	2.7466e-01	1.3097e+00	4.7685e+00	2.4339e+00	7.7311e+00
0.25	2.8588e-01	1.3076e+00	4.5741e+00	2.3440e+00	6.9800e+00
0.26	2.9706e-01	1.3054e+00	4.3945e+00	2.2614e+00	6.3186e+00
0.27	3.0822e-01	1.3032e+00	4.2280e+00	2.1852e+00	5.7335e+00
0.28	3.1935e-01	1.3008e+00	4.0734e+00	2.1147e+00	5.2140e+00
0.29	3.3045e-01	1.2984e+00	3.9292e+00	2.0494e+00	4.7510e+00
0.30	3.4152e-01	1.2959e+00	3.7946e+00	1.9886e+00	4.3369e+00
0.31	3.5255e-01	1.2934e+00	3.6686e+00	1.9321e+00	3.9654e+00
0.32	3.6355e-01	1.2907e+00	3.5503e+00	1.8794e+00	3.6312e+00
0.33	3.7452e-01	1.2880e+00	3.4391e+00	1.8301e+00	3.3296e+00
0.34	3.8545e-01	1.2852e+00	3.3344e+00	1.7839e+00	3.0569e+00
0.35	3.9635e-01	1.2824e+00	3.2355e+00	1.7406e+00	2.8097e+00
0.36	4.0721e-01	1.2795e+00	3.1420e+00	1.7000e+00	2.5852e+00
0.37	4.1803e-01	1.2765e+00	3.0535e+00	1.6618e+00	2.3807e+00
0.38	4.2881e-01	1.2734e+00	2.9696e+00	1.6258e+00	2.1943e+00
0.39	4.3956e-01	1.2703e+00	2.8899e+00	1.5919e+00	2.0239e+00
0.40	4.5026e-01	1.2671e+00	2.8141e+00	1.5599e+00	1.8680e+00
0.41	4.6092e-01	1.2638e+00	2.7420e+00	1.5297e+00	1.7251e+00
0.42	4.7154e-01	1.2605e+00	2.6732e+00	1.5011e+00	1.5939e+00
0.43	4.8212e-01	1.2571e+00	2.6075e+00	1.4740e+00	1.4733e+00
0.44	4.9266e-01	1.2537e+00	2.5447e+00	1.4484e+00	1.3623e+00
0.45	5.0315e-01	1.2502e+00	2.4847e+00	1.4242e+00	1.2601e+00
0.46	5.1360e-01	1.2466e+00	2.4272e+00	1.4011e+00	1.1658e+00
0.47	5.2401e-01	1.2430e+00	2.3721e+00	1.3793e+00	1.0787e+00
0.48	5.3436e-01	1.2393e+00	2.3193e+00	1.3585e+00	9.9823e-01
0.49	5.4468e-01	1.2356e+00	2.2685e+00	1.3388e+00	9.2379e-01
0.50	5.5494e-01	1.2318e+00	2.2198e+00	1.3201e+00	8.5488e-01

Table C.1. Fanno Flow (γ=1.67) (cont.)

M	$M^* = \frac{\rho^*}{\rho}$	$\frac{T}{T^*}$	$\frac{P}{P^*}$	$\frac{P_t}{P_t^*}$	$\frac{4fL^*}{D}$
0.51	5.6516e-01	1.2280e+00	2.1728e+00	1.3023e+00	7.9104e-01
0.52	5.7533e-01	1.2241e+00	2.1277e+00	1.2853e+00	7.3186e-01
0.53	5.8545e-01	1.2202e+00	2.0842e+00	1.2692e+00	6.7696e-01
0.54	5.9552e-01	1.2162e+00	2.0422e+00	1.2538e+00	6.2601e-01
0.55	6.0554e-01	1.2122e+00	2.0018e+00	1.2392e+00	5.7870e-01
0.56	6.1551e-01	1.2081e+00	1.9627e+00	1.2253e+00	5.3474e-01
0.57	6.2543e-01	1.2040e+00	1.9250e+00	1.2120e+00	4.9390e-01
0.58	6.3530e-01	1.1998e+00	1.8885e+00	1.1994e+00	4.5593e-01
0.59	6.4512e-01	1.1956e+00	1.8533e+00	1.1873e+00	4.2062e-01
0.60	6.5489e-01	1.1913e+00	1.8191e+00	1.1759e+00	3.8778e-01
0.61	6.6460e-01	1.1870e+00	1.7861e+00	1.1649e+00	3.5723e-01
0.62	6.7426e-01	1.1827e+00	1.7541e+00	1.1545e+00	3.2881e-01
0.63	6.8387e-01	1.1783e+00	1.7230e+00	1.1446e+00	3.0237e-01
0.64	6.9342e-01	1.1739e+00	1.6929e+00	1.1352e+00	2.7778e-01
0.65	7.0292e-01	1.1695e+00	1.6637e+00	1.1262e+00	2.5490e-01
0.66	7.1237e-01	1.1650e+00	1.6354e+00	1.1176e+00	2.3361e-01
0.67	7.2176e-01	1.1605e+00	1.6078e+00	1.1095e+00	2.1383e-01
0.68	7.3110e-01	1.1559e+00	1.5811e+00	1.1018e+00	1.9543e-01
0.69	7.4038e-01	1.1514e+00	1.5551e+00	1.0944e+00	1.7834e-01
0.70	7.4961e-01	1.1468e+00	1.5298e+00	1.0874e+00	1.6246e-01
0.71	7.5878e-01	1.1421e+00	1.5052e+00	1.0808e+00	1.4772e-01
0.72	7.6789e-01	1.1375e+00	1.4813e+00	1.0745e+00	1.3405e-01
0.73	7.7695e-01	1.1328e+00	1.4580e+00	1.0685e+00	1.2137e-01
0.74	7.8596e-01	1.1281e+00	1.4353e+00	1.0629e+00	1.0962e-01
0.75	7.9490e-01	1.1233e+00	1.4132e+00	1.0576e+00	9.8752e-02
0.76	8.0379e-01	1.1186e+00	1.3916e+00	1.0525e+00	8.8704e-02
0.77	8.1263e-01	1.1138e+00	1.3706e+00	1.0478e+00	7.9425e-02
0.78	8.2140e-01	1.1090e+00	1.3501e+00	1.0433e+00	7.0869e-02
0.79	8.3012e-01	1.1042e+00	1.3301e+00	1.0391e+00	6.2992e-02
0.80	8.3878e-01	1.0993e+00	1.3106e+00	1.0351e+00	5.5752e-02
0.81	8.4739e-01	1.0944e+00	1.2916e+00	1.0314e+00	4.9111e-02
0.82	8.5594e-01	1.0896e+00	1.2730e+00	1.0279e+00	4.3034e-02
0.83	8.6443e-01	1.0847e+00	1.2548e+00	1.0247e+00	3.7486e-02
0.84	8.7286e-01	1.0798e+00	1.2370e+00	1.0217e+00	3.2435e-02
0.85	8.8124e-01	1.0748e+00	1.2197e+00	1.0189e+00	2.7853e-02
0.86	8.8955e-01	1.0699e+00	1.2028e+00	1.0163e+00	2.3712e-02
0.87	8.9782e-01	1.0650e+00	1.1862e+00	1.0139e+00	1.9986e-02
0.88	9.0602e-01	1.0600e+00	1.1700e+00	1.0118e+00	1.6651e-02
0.89	9.1417e-01	1.0550e+00	1.1541e+00	1.0098e+00	1.3683e-02
0.90	9.2225e-01	1.0501e+00	1.1386e+00	1.0081e+00	1.1061e-02
0.91	9.3029e-01	1.0451e+00	1.1234e+00	1.0065e+00	8.7662e-03
0.92	9.3826e-01	1.0401e+00	1.1085e+00	1.0051e+00	6.7781e-03
0.93	9.4618e-01	1.0351e+00	1.0940e+00	1.0039e+00	5.0795e-03
0.94	9.5404e-01	1.0301e+00	1.0797e+00	1.0028e+00	3.6535e-03
0.95	9.6184e-01	1.0251e+00	1.0657e+00	1.0019e+00	2.4843e-03
0.96	9.6958e-01	1.0201e+00	1.0521e+00	1.0012e+00	1.5572e-03
0.97	9.7727e-01	1.0151e+00	1.0387e+00	1.0007e+00	8.5802e-04
0.98	9.8491e-01	1.0100e+00	1.0255e+00	1.0003e+00	3.7362e-04
0.99	9.9248e-01	1.0050e+00	1.0126e+00	1.0001e+00	9.1530e-05
1.00	1.0000e+00	1.0000e+00	1.0000e+00	1.0000e+00	0.0000e+00

APPENDIX D. ISOTHERMAL FANNO FLOW PROPERTIES

A. EQUATIONS

1. Dimensionless velocity

$$\frac{V}{V^*}=\frac{P^*}{P}=\sqrt{\gamma}M$$

2. Critical stagnation pressure ratio

$$\frac{P_t}{P_t^*}=\frac{1}{\sqrt{\gamma}M}\left\{\left[\frac{2\gamma}{3\gamma-1}\right]\left[1+\frac{\gamma-1}{2}M^2\right]\right\}^{\frac{\gamma}{\gamma-1}}$$

3. Critical stagnation temperature ratio

$$\frac{T_t}{T_t^*}=\left[\frac{2\gamma}{3\gamma-1}\right]\left[1+\frac{\gamma-1}{2}M^2\right]$$

4. Critical length ratio

$$\frac{4fL^*}{D}=\frac{1-\gamma M^2}{\gamma M^2}+\ln\left(\gamma M^2\right)$$

B. MATLAB CODE

```
% iFanno.m
%
% Fanno flow parameters (isothermal flow)
%
% Variables:
%
%           M - Mach Number
%           k - Gamma (Specific Heat Ratio)
%        PRAT - Static Pressure Ratio
%     BIGTRAT - Stagnation Temperature Ratio
%     BIGPRAT - Stagnation Pressure Ratio
%      FLDRAT - Critical Length Ratio
%
M1 = [0:.01:.77];
M2 = [.78:.01:1];
M = [M1 1/sqrt(1.67) M2];

k = 1.67;

PRAT = sqrt(k).*M;

BIGTRAT = (((2*k)/((3*k)-1))*(1+(((k-1)/2).*M.^2)));

BIGPRAT = (1./PRAT).*((BIGTRAT).^(k/(k-1)));

FLDRAT = (1-(k.*(M.^2))./(k.*(M.^2))+log(k.*(M.^2));

Y=[M;PRAT;BIGTRAT;BIGPRAT;FLDRAT];

fid = fopen('ifanno.txt','w');
fprintf(fid,'%2.2f\t %4.4e\t %4.4e\t %4.4e\t %4.4e\n',Y);
fclose(fid);
```

Table D.1. Isothermal Fanno Flow (γ=1.67)

M	$\frac{V}{V^\star}=\frac{P^\star}{P}$	$\frac{P_t}{P_t^\star}$	$\frac{T_t}{T_t^\star}$	$\frac{4fL^\star}{D}$
0.00	0.0000e+00	8.3292e-01	∞	∞
0.01	1.2923e-02	8.3295e-01	4.9065e+01	5.9783e+03
0.02	2.5846e-02	8.3303e-01	2.4539e+01	1.4887e+03
0.03	3.8769e-02	8.3317e-01	1.6366e+01	6.5784e+02
0.04	5.1691e-02	8.3336e-01	1.2282e+01	3.6733e+02
0.05	6.4614e-02	8.3362e-01	9.8328e+00	2.3304e+02
0.06	7.7537e-02	8.3392e-01	8.2015e+00	1.6022e+02
0.07	9.0460e-02	8.3428e-01	7.0375e+00	1.1640e+02
0.08	1.0338e-01	8.3470e-01	6.1655e+00	8.8024e+01
0.09	1.1631e-01	8.3518e-01	5.4882e+00	6.8623e+01
0.10	1.2923e-01	8.3571e-01	4.9472e+00	5.4788e+01
0.11	1.4215e-01	8.3629e-01	4.5053e+00	4.4586e+01
0.12	1.5507e-01	8.3694e-01	4.1378e+00	3.6856e+01
0.13	1.6800e-01	8.3763e-01	3.8274e+00	3.0864e+01
0.14	1.8092e-01	8.3839e-01	3.5620e+00	2.6132e+01
0.15	1.9384e-01	8.3920e-01	3.3326e+00	2.2332e+01
0.16	2.0677e-01	8.4006e-01	3.1323e+00	1.9238e+01
0.17	2.1969e-01	8.4098e-01	2.9561e+00	1.6689e+01
0.18	2.3261e-01	8.4196e-01	2.8000e+00	1.4565e+01
0.19	2.4553e-01	8.4299e-01	2.6607e+00	1.2779e+01
0.20	2.5846e-01	8.4408e-01	2.5358e+00	1.1264e+01
0.21	2.7138e-01	8.4522e-01	2.4232e+00	9.9698e+00
0.22	2.8430e-01	8.4642e-01	2.3213e+00	8.8565e+00
0.23	2.9723e-01	8.4768e-01	2.2286e+00	7.8930e+00
0.24	3.1015e-01	8.4899e-01	2.1440e+00	7.0545e+00
0.25	3.2307e-01	8.5036e-01	2.0665e+00	6.3211e+00
0.26	3.3599e-01	8.5178e-01	1.9953e+00	5.6767e+00
0.27	3.4892e-01	8.5326e-01	1.9297e+00	5.1082e+00
0.28	3.6184e-01	8.5479e-01	1.8692e+00	4.6047e+00
0.29	3.7476e-01	8.5638e-01	1.8131e+00	4.1572e+00
0.30	3.8769e-01	8.5803e-01	1.7611e+00	3.7582e+00
0.31	4.0061e-01	8.5973e-01	1.7127e+00	3.4015e+00
0.32	4.1353e-01	8.6149e-01	1.6676e+00	3.0816e+00
0.33	4.2645e-01	8.6330e-01	1.6256e+00	2.7941e+00
0.34	4.3938e-01	8.6517e-01	1.5863e+00	2.5352e+00
0.35	4.5230e-01	8.6710e-01	1.5496e+00	2.3014e+00
0.36	4.6522e-01	8.6908e-01	1.5151e+00	2.0899e+00
0.37	4.7815e-01	8.7112e-01	1.4828e+00	1.8983e+00
0.38	4.9107e-01	8.7321e-01	1.4524e+00	1.7245e+00
0.39	5.0399e-01	8.7536e-01	1.4239e+00	1.5665e+00
0.40	5.1691e-01	8.7756e-01	1.3970e+00	1.4228e+00
0.41	5.2984e-01	8.7982e-01	1.3717e+00	1.2918e+00
0.42	5.4276e-01	8.8214e-01	1.3478e+00	1.1724e+00
0.43	5.5568e-01	8.8451e-01	1.3253e+00	1.0634e+00
0.44	5.6861e-01	8.8694e-01	1.3041e+00	9.6385e-01
0.45	5.8153e-01	8.8942e-01	1.2840e+00	8.7286e-01
0.46	5.9445e-01	8.9196e-01	1.2651e+00	7.8965e-01
0.47	6.0737e-01	8.9455e-01	1.2472e+00	7.1352e-01
0.48	6.2030e-01	8.9721e-01	1.2302e+00	6.4385e-01
0.49	6.3322e-01	8.9991e-01	1.2142e+00	5.8009e-01
0.50	6.4614e-01	9.0267e-01	1.1990e+00	5.2174e-01

Table D.1. Isothermal Fanno Flow (γ=1.67) (cont.)

M	$\frac{V}{V^*}=\frac{P^*}{P}$	$\frac{P_t}{P_t^*}$	$\frac{T_t}{T_t^*}$	$\frac{4fL^*}{D}$
0.51	6.5907e-01	9.0549e-01	1.1847e+00	4.6834e-01
0.52	6.7199e-01	9.0837e-01	1.1711e+00	4.1948e-01
0.53	6.8491e-01	9.1130e-01	1.1583e+00	3.7480e-01
0.54	6.9783e-01	9.1428e-01	1.1461e+00	3.3396e-01
0.55	7.1076e-01	9.1732e-01	1.1347e+00	2.9666e-01
0.56	7.2368e-01	9.2042e-01	1.1238e+00	2.6263e-01
0.57	7.3660e-01	9.2357e-01	1.1135e+00	2.3162e-01
0.58	7.4953e-01	9.2678e-01	1.1038e+00	2.0340e-01
0.59	7.6245e-01	9.3005e-01	1.0947e+00	1.7776e-01
0.60	7.7537e-01	9.3337e-01	1.0860e+00	1.5451e-01
0.61	7.8829e-01	9.3674e-01	1.0779e+00	1.3348e-01
0.62	8.0122e-01	9.4018e-01	1.0702e+00	1.1451e-01
0.63	8.1414e-01	9.4366e-01	1.0630e+00	9.7451e-02
0.64	8.2706e-01	9.4721e-01	1.0562e+00	8.2169e-02
0.65	8.3999e-01	9.5081e-01	1.0498e+00	6.8542e-02
0.66	8.5291e-01	9.5446e-01	1.0439e+00	5.6454e-02
0.67	8.6583e-01	9.5817e-01	1.0383e+00	4.5801e-02
0.68	8.7875e-01	9.6194e-01	1.0331e+00	3.6487e-02
0.69	8.9168e-01	9.6576e-01	1.0282e+00	2.8420e-02
0.70	9.0460e-01	9.6964e-01	1.0237e+00	2.1519e-02
0.71	9.1752e-01	9.7358e-01	1.0195e+00	1.5707e-02
0.72	9.3045e-01	9.7757e-01	1.0157e+00	1.0913e-02
0.73	9.4337e-01	9.8161e-01	1.0121e+00	7.0696e-03
0.74	9.5629e-01	9.8571e-01	1.0089e+00	4.1167e-03
0.75	9.6921e-01	9.8987e-01	1.0059e+00	1.9971e-03
0.76	9.8214e-01	9.9408e-01	1.0032e+00	6.5768e-04
0.77	9.9506e-01	9.9835e-01	1.0008e+00	4.9226e-05
0.77	1.0000e+00	1.0000e+00	1.0000e+00	0.0000e+00
0.78	1.0080e+00	1.0027e+00	9.9872e-01	1.2575e-04
0.79	1.0209e+00	1.0071e+00	9.9685e-01	8.4442e-04
0.80	1.0338e+00	1.0115e+00	9.9523e-01	2.1653e-03
0.81	1.0468e+00	1.0160e+00	9.9386e-01	4.0510e-03
0.82	1.0597e+00	1.0205e+00	9.9273e-01	6.4667e-03
0.83	1.0726e+00	1.0251e+00	9.9184e-01	9.3797e-03
0.84	1.0855e+00	1.0298e+00	9.9117e-01	1.2760e-02
0.85	1.0984e+00	1.0345e+00	9.9073e-01	1.6578e-02
0.86	1.1114e+00	1.0393e+00	9.9050e-01	2.0808e-02
0.87	1.1243e+00	1.0441e+00	9.9049e-01	2.5424e-02
0.88	1.1372e+00	1.0490e+00	9.9069e-01	3.0404e-02
0.89	1.1501e+00	1.0539e+00	9.9110e-01	3.5724e-02
0.90	1.1631e+00	1.0589e+00	9.9170e-01	4.1365e-02
0.91	1.1760e+00	1.0640e+00	9.9251e-01	4.7306e-02
0.92	1.1889e+00	1.0691e+00	9.9350e-01	5.3530e-02
0.93	1.2018e+00	1.0742e+00	9.9469e-01	6.0019e-02
0.94	1.2147e+00	1.0795e+00	9.9607e-01	6.6758e-02
0.95	1.2277e+00	1.0847e+00	9.9763e-01	7.3730e-02
0.96	1.2406e+00	1.0901e+00	9.9937e-01	8.0922e-02
0.97	1.2535e+00	1.0955e+00	1.0013e+00	8.8320e-02
0.98	1.2664e+00	1.1009e+00	1.0034e+00	9.5911e-02
0.99	1.2794e+00	1.1064e+00	1.0057e+00	1.0368e-01
1.00	1.2923e+00	1.1119e+00	1.0081e+00	1.1163e-01

APPENDIX E. RAYLEIGH FLOW PROPERTIES

A. EQUATIONS

1. Dimensionless velocity

$$M^{\star}=\frac{\rho^{\star}}{\rho}=\frac{(\gamma+1)M^2}{1+\gamma M^2}$$

2. Critical temperature ratio

$$\frac{T}{T^{\star}}=\frac{(\gamma+1)^2M^2}{\left(1+\gamma M^2\right)^2}$$

3. Critical pressure ratio

$$\frac{P}{P^{\star}}=\frac{\gamma+1}{1+\gamma M^2}$$

4. Critical stagnation pressure ratio

$$\frac{P_t}{P_t^{\star}}=\frac{\gamma+1}{1+\gamma M^2}\left\{\left[\frac{2}{\gamma+1}\right]\left[1+\frac{\gamma-1}{2}M^2\right]\right\}^{\frac{\gamma}{\gamma-1}}$$

5. Critical stagnation temperature ratio

$$\frac{T_t}{T_t^{\star}}=\frac{2(\gamma+1)M^2}{\left(1+\gamma M^2\right)^2}\left[1+\frac{\gamma-1}{2}M^2\right]$$

B. MATLAB CODE

```
% Rayleigh.m
%
% Rayleigh flow parameters
%
% Variables:
%
%           M - Mach Number
%           k - Gamma (Specific Heat Ratio)
%       MSTAR - Dimensionless Velocity
%        TRAT - Static Temperature Ratio
%        PRAT - Static Pressure Ratio
%     BIGPRAT - Stagnation Pressure Ratio
%     BIGTRAT - Stagnation Temperature Ratio
%
M = [0:.01:1];

k = 1.67;

MSTAR = ((k+1).*(M.^2))./(1+(k.*(M.^2)));

TRAT = ((k+1)^2).*(M.^2)./((1+(k.*(M.^2))).^2);

PRAT = (k+1)./(1+(k.*(M.^2)));

BIGPRAT = (PRAT).*(((2/(k+1))*(1+(((k-1)/2).*M.^2))).^(k/(k-1)));

BIGTRAT = ((2*(k+1).*(M.^2))./((1+(k.*(M.^2))).^2).*(1+ ...
          (((k-1)/2).*M.^2)));

Y=[M;MSTAR;TRAT;PRAT;BIGPRAT;BIGTRAT];

fid = fopen('rayleigh.txt','w');
fprintf(fid,'%2.2f\t %4.4e\t %4.4e\t %4.4e\t %4.4e\t %4.4e\n',Y);
fclose(fid);
```

Table E.1. Rayleigh Flow (γ=1.67)

M	$M^\star=\frac{\rho^\star}{\rho}$	$\frac{T}{T^\star}$	$\frac{P}{P^\star}$	$\frac{P_t}{P_t^\star}$	$\frac{T_t}{T_t^\star}$
0.00	0.0000e+00	0.0000e+00	2.6700e+00	1.2994e+00	0.0000e+00
0.01	2.6696e-04	7.1265e-04	2.6696e+00	1.2993e+00	5.3384e-04
0.02	1.0673e-03	2.8478e-03	2.6682e+00	1.2990e+00	2.1334e-03
0.03	2.3994e-03	6.3968e-03	2.6660e+00	1.2984e+00	4.7930e-03
0.04	4.2606e-03	1.1346e-02	2.6629e+00	1.2977e+00	8.5031e-03
0.05	6.6472e-03	1.7674e-02	2.6589e+00	1.2967e+00	1.3250e-02
0.06	9.5546e-03	2.5358e-02	2.6540e+00	1.2955e+00	1.9018e-02
0.07	1.2977e-02	3.4367e-02	2.6483e+00	1.2941e+00	2.5785e-02
0.08	1.6907e-02	4.4665e-02	2.6418e+00	1.2925e+00	3.3529e-02
0.09	2.1338e-02	5.6213e-02	2.6344e+00	1.2908e+00	4.2221e-02
0.10	2.6261e-02	6.8966e-02	2.6261e+00	1.2888e+00	5.1833e-02
0.11	3.1667e-02	8.2876e-02	2.6171e+00	1.2866e+00	6.2331e-02
0.12	3.7545e-02	9.7891e-02	2.6073e+00	1.2842e+00	7.3681e-02
0.13	4.3884e-02	1.1396e-01	2.5967e+00	1.2816e+00	8.5843e-02
0.14	5.0673e-02	1.3101e-01	2.5854e+00	1.2789e+00	9.8779e-02
0.15	5.7899e-02	1.4899e-01	2.5733e+00	1.2760e+00	1.1245e-01
0.16	6.5550e-02	1.6784e-01	2.5605e+00	1.2729e+00	1.2680e-01
0.17	7.3610e-02	1.8749e-01	2.5471e+00	1.2697e+00	1.4180e-01
0.18	8.2067e-02	2.0787e-01	2.5329e+00	1.2663e+00	1.5740e-01
0.19	9.0907e-02	2.2892e-01	2.5182e+00	1.2628e+00	1.7355e-01
0.20	1.0011e-01	2.5056e-01	2.5028e+00	1.2591e+00	1.9020e-01
0.21	1.0967e-01	2.7273e-01	2.4869e+00	1.2553e+00	2.0731e-01
0.22	1.1956e-01	2.9536e-01	2.4703e+00	1.2514e+00	2.2483e-01
0.23	1.2978e-01	3.1838e-01	2.4533e+00	1.2474e+00	2.4271e-01
0.24	1.4030e-01	3.4172e-01	2.4357e+00	1.2432e+00	2.6091e-01
0.25	1.5110e-01	3.6532e-01	2.4177e+00	1.2390e+00	2.7937e-01
0.26	1.6218e-01	3.8910e-01	2.3992e+00	1.2346e+00	2.9806e-01
0.27	1.7352e-01	4.1301e-01	2.3802e+00	1.2302e+00	3.1693e-01
0.28	1.8509e-01	4.3699e-01	2.3609e+00	1.2257e+00	3.3593e-01
0.29	1.9689e-01	4.6097e-01	2.3412e+00	1.2211e+00	3.5502e-01
0.30	2.0890e-01	4.8489e-01	2.3211e+00	1.2164e+00	3.7416e-01
0.31	2.2110e-01	5.0870e-01	2.3008e+00	1.2117e+00	3.9332e-01
0.32	2.3348e-01	5.3236e-01	2.2801e+00	1.2070e+00	4.1245e-01
0.33	2.4602e-01	5.5580e-01	2.2591e+00	1.2022e+00	4.3152e-01
0.34	2.5871e-01	5.7898e-01	2.2380e+00	1.1973e+00	4.5049e-01
0.35	2.7153e-01	6.0185e-01	2.2165e+00	1.1925e+00	4.6933e-01
0.36	2.8446e-01	6.2438e-01	2.1949e+00	1.1876e+00	4.8801e-01
0.37	2.9751e-01	6.4653e-01	2.1732e+00	1.1827e+00	5.0650e-01
0.38	3.1064e-01	6.6826e-01	2.1512e+00	1.1778e+00	5.2478e-01
0.39	3.2385e-01	6.8953e-01	2.1292e+00	1.1728e+00	5.4282e-01
0.40	3.3712e-01	7.1032e-01	2.1070e+00	1.1679e+00	5.6059e-01
0.41	3.5045e-01	7.3060e-01	2.0848e+00	1.1630e+00	5.7808e-01
0.42	3.6381e-01	7.5034e-01	2.0624e+00	1.1581e+00	5.9527e-01
0.43	3.7721e-01	7.6953e-01	2.0401e+00	1.1533e+00	6.1213e-01
0.44	3.9062e-01	7.8814e-01	2.0177e+00	1.1484e+00	6.2866e-01
0.45	4.0404e-01	8.0616e-01	1.9953e+00	1.1436e+00	6.4483e-01
0.46	4.1746e-01	8.2358e-01	1.9729e+00	1.1388e+00	6.6064e-01
0.47	4.3086e-01	8.4037e-01	1.9505e+00	1.1341e+00	6.7608e-01
0.48	4.4424e-01	8.5655e-01	1.9281e+00	1.1294e+00	6.9113e-01
0.49	4.5759e-01	8.7209e-01	1.9058e+00	1.1248e+00	7.0579e-01
0.50	4.7090e-01	8.8699e-01	1.8836e+00	1.1202e+00	7.2005e-01

Table E.1. Rayleigh Flow (γ=1.67) (cont.)

M	$M^* = \frac{\rho^*}{\rho}$	$\frac{T}{T^*}$	$\frac{P}{P^*}$	$\frac{P_t}{P_t^*}$	$\frac{T_t}{T_t^*}$
0.51	4.8416e-01	9.0124e-01	1.8614e+00	1.1156e+00	7.3391e-01
0.52	4.9737e-01	9.1486e-01	1.8394e+00	1.1112e+00	7.4736e-01
0.53	5.1052e-01	9.2783e-01	1.8174e+00	1.1067e+00	7.6041e-01
0.54	5.2360e-01	9.4017e-01	1.7956e+00	1.1024e+00	7.7304e-01
0.55	5.3660e-01	9.5186e-01	1.7739e+00	1.0981e+00	7.8526e-01
0.56	5.4952e-01	9.6293e-01	1.7523e+00	1.0939e+00	7.9707e-01
0.57	5.6236e-01	9.7336e-01	1.7309e+00	1.0898e+00	8.0847e-01
0.58	5.7510e-01	9.8318e-01	1.7096e+00	1.0857e+00	8.1946e-01
0.59	5.8775e-01	9.9239e-01	1.6885e+00	1.0817e+00	8.3005e-01
0.60	6.0030e-01	1.0010e+00	1.6675e+00	1.0778e+00	8.4024e-01
0.61	6.1274e-01	1.0090e+00	1.6467e+00	1.0740e+00	8.5003e-01
0.62	6.2508e-01	1.0165e+00	1.6261e+00	1.0703e+00	8.5943e-01
0.63	6.3730e-01	1.0233e+00	1.6057e+00	1.0667e+00	8.6845e-01
0.64	6.4941e-01	1.0296e+00	1.5855e+00	1.0631e+00	8.7709e-01
0.65	6.6140e-01	1.0354e+00	1.5655e+00	1.0597e+00	8.8535e-01
0.66	6.7328e-01	1.0406e+00	1.5456e+00	1.0563e+00	8.9325e-01
0.67	6.8503e-01	1.0454e+00	1.5260e+00	1.0530e+00	9.0079e-01
0.68	6.9665e-01	1.0496e+00	1.5066e+00	1.0499e+00	9.0798e-01
0.69	7.0815e-01	1.0533e+00	1.4874e+00	1.0468e+00	9.1482e-01
0.70	7.1952e-01	1.0565e+00	1.4684e+00	1.0438e+00	9.2133e-01
0.71	7.3076e-01	1.0593e+00	1.4496e+00	1.0409e+00	9.2751e-01
0.72	7.4187e-01	1.0617e+00	1.4311e+00	1.0381e+00	9.3337e-01
0.73	7.5285e-01	1.0636e+00	1.4127e+00	1.0354e+00	9.3892e-01
0.74	7.6370e-01	1.0651e+00	1.3946e+00	1.0328e+00	9.4416e-01
0.75	7.7441e-01	1.0662e+00	1.3767e+00	1.0303e+00	9.4911e-01
0.76	7.8499e-01	1.0669e+00	1.3591e+00	1.0279e+00	9.5377e-01
0.77	7.9544e-01	1.0672e+00	1.3416e+00	1.0256e+00	9.5816e-01
0.78	8.0576e-01	1.0671e+00	1.3244e+00	1.0234e+00	9.6227e-01
0.79	8.1594e-01	1.0667e+00	1.3074e+00	1.0213e+00	9.6612e-01
0.80	8.2599e-01	1.0660e+00	1.2906e+00	1.0193e+00	9.6972e-01
0.81	8.3590e-01	1.0650e+00	1.2740e+00	1.0174e+00	9.7307e-01
0.82	8.4568e-01	1.0636e+00	1.2577e+00	1.0156e+00	9.7619e-01
0.83	8.5533e-01	1.0620e+00	1.2416e+00	1.0139e+00	9.7907e-01
0.84	8.6485e-01	1.0600e+00	1.2257e+00	1.0123e+00	9.8174e-01
0.85	8.7424e-01	1.0578e+00	1.2100e+00	1.0108e+00	9.8418e-01
0.86	8.8350e-01	1.0554e+00	1.1946e+00	1.0094e+00	9.8643e-01
0.87	8.9262e-01	1.0527e+00	1.1793e+00	1.0081e+00	9.8847e-01
0.88	9.0162e-01	1.0497e+00	1.1643e+00	1.0069e+00	9.9032e-01
0.89	9.1050e-01	1.0466e+00	1.1495e+00	1.0058e+00	9.9199e-01
0.90	9.1924e-01	1.0432e+00	1.1349e+00	1.0048e+00	9.9348e-01
0.91	9.2786e-01	1.0396e+00	1.1205e+00	1.0039e+00	9.9480e-01
0.92	9.3636e-01	1.0359e+00	1.1063e+00	1.0030e+00	9.9595e-01
0.93	9.4473e-01	1.0319e+00	1.0923e+00	1.0023e+00	9.9695e-01
0.94	9.5298e-01	1.0278e+00	1.0785e+00	1.0017e+00	9.9779e-01
0.95	9.6111e-01	1.0235e+00	1.0649e+00	1.0012e+00	9.9849e-01
0.96	9.6912e-01	1.0191e+00	1.0516e+00	1.0008e+00	9.9905e-01
0.97	9.7702e-01	1.0145e+00	1.0384e+00	1.0004e+00	9.9947e-01
0.98	9.8479e-01	1.0098e+00	1.0254e+00	1.0002e+00	9.9977e-01
0.99	9.9245e-01	1.0050e+00	1.0126e+00	1.0000e+00	9.9994e-01
1.00	1.0000e+00	1.0000e+00	1.0000e+00	1.0000e+00	1.0000e+00

APPENDIX F. FLOW CALCULATION CODE

```
% flowcalc.m
%
% A program to estimate the theoretical performance of a thermothrottle
% as a function of temperature for various values of throttle length
% and diameter and inlet pressure.
%
% Initial Conditions
Tt0 = 275;
Tt2 = Tt0;
for Tt3 = 275:10:375;
Pt0 = 10000;
Pt1 = Pt0;
L1 = .5;
L2 = .1;
L3 = .9;
D = .003;
A = (pi*(D^2))/4;
k = 1.67;
R = 63.323;
%
% Isentropic Flow to Station 1
%
rho0 = Pt0/(R*Tt0);
Vstar = sqrt(((2*k)/(k+1))*R*Tt0);
rho0star = rho0*((2/(k+1))^(1/(k-1)));
mdotstari = rho0star*A*Vstar;
%
% Fanno Flow to Station 2
%
f = ((48*pi)/1E8)*(2.146/mdotstari);
yT = (4*f*(L1+L2+L3))/D;
M1 = sqrt((1+(yT/2)-(sqrt((25*yT^2)+(100*yT)+10)/10))/k);
rho1 = rho0/((1+((k-1)/2)*(M1^2))^(k/(k-1)));
rho1star = rho1*sqrt(k)*M1;
mdotstarf = rho1star*A*Vstar;
f1 = f;
y1 = yT-((4*f1*L1)/D);
M2 = sqrt((1+(y1/2)-(sqrt((25*y1^2)+(100*y1)+10)/10))/k);
Pt2 = Pt1*((1/(sqrt(k)*M2))*(((((2*k)/((3*k)-1))*...
      (1+(((k-1)/2)*M2^2))))^(k/(k-1))))/((1/(sqrt(k)*M1))*...
      (((((2*k)/((3*k)-1))*(1+(((k-1)/2)*M1^2))))^(k/(k-1))));
%
% Rayleigh Flow to Station 3
%
```

```
TtRatio1 = (Tt3/Tt2)*...
           ((2*(k+1)*(M2^2))/((1+(k*(M2^2)))^2)*(1+(((k-1)/2)*M2^2)));
z1 = TtRatio1;
M3 = sqrt(((-sqrt(-((k^2)*z1)-(2*k*z1)+(k^2)+(2*k)+1-z1))...
     -(k*z1)+k+1)/(((k^2)*z1)-(k^2)+1));
Pt3 = Pt2*(((k+1)/(1+(k*(M3^2))))*(((2/(k+1))*...
      (1+(((k-1)/2)*M3^2)))^(k/(k-1))))/(((k+1)/(1+(k*(M2^2))))*...
      (((2/(k+1))*(1+(((k-1)/2)*M2^2)))^(k/(k-1))));
rho3 = Pt3/(R*Tt3);
rho3star = rho3*(((k+1)*(M3^2))/(1+(k*(M3^2))));
mdot3star = rho3star*A*Vstar;
%
% Fanno Flow to Station 4
%
f3 = ((48*pi)/1E8)*((2.146+(.00714*(Tt3-275)))/mdot3star);
y3 = (4*f3*L3)/D;
%
% Station 4 to Station 1 (and back)
%
f3a = f3;
y3a = y3;
M3a = sqrt((1+(y3a/2)-(sqrt((25*y3a^2)+(100*y3a)+10)/10))/k);
TtRatio2 = (Tt2/Tt3)*((2*(k+1)*(M3a^2))/((1+(k*(M3a^2)))^2)*...
           (1+(((k-1)/2)*M3a^2)));
z2 = TtRatio2;
M2a = sqrt(((-sqrt(-((k^2)*z2)-(2*k*z2)+(k^2)+(2*k)+1-z2))...
      -(k*z2)+k+1)/(((k^2)*z2)-(k^2)+1));
f1a = ((48*pi)/1E8)*(2.146/mdot3star);
y1a = log(k*(M2a^2))+((1-(k*(M2a^2)))/(k*(M2a^2)))+((4*f1a*L1)/D);
M1a = sqrt((1+(y1a/2)-(sqrt((25*y1a^2)+(100*y1a)+10)/10))/k);
Pt2a = Pt1*((1/(sqrt(k)*M2a))*(((((2*k)/((3*k)-1))*...
       (1+(((k-1)/2)*M2a^2))))^(k/(k-1))))/((1/(sqrt(k)*M1a))*...
       (((((2*k)/((3*k)-1))*(1+(((k-1)/2)*M1a^2))))^(k/(k-1))));
Pt3a = Pt2a*(((k+1)/(1+(k*(M3a^2))))*(((2/(k+1))*...
       (1+(((k-1)/2)*M3a^2)))^(k/(k-1))))/(((k+1)/(1+(k*(M2a^2))))*...
       (((2/(k+1))*(1+(((k-1)/2)*M2a^2)))^(k/(k-1))));
rho3a = Pt3a/(R*Tt3);
rho3astar = rho3a*(((k+1)*(M3a^2))/(1+(k*(M3a^2))));
%
% Theoretical mass flow rate
%
mdot3astar = rho3astar*A*Vstar
f1b = ((48*pi)/1E8)*(2.146/mdot3star);
y1b = (4*f1b*L1)/D;
f3b = ((48*pi)/1E8)*((2.146+(.00714*(Tt3-275)))/mdot3astar);
y3b = (4*f3b*L3)/D;
end
```

LIST OF REFERENCES

Agrawal, B. N., *Design of Geosynchronous Spacecraft*, Prentice-Hall, Inc., 1986.

Biblarz, O. and Andrews, J. R., "Temperature Dependence of Gas Properties in Polynomial Form," Naval Postgraduate School Report NPS67-81-001, January 1981.

Brophy, J. R., "Stationary Plasma Thruster Evaluation in Russia," JPL Publication 92-4, March 15, 1992.

Cann, G. L., assignor to Electro-Optical Systems, Inc., U.S. Patent 3243954, "Plasma Accelerator Using Hall Currents," patented April 5, 1966, filed August 17, 1962, Ser. No. 217631.

Cann, G. L., assignor to Electro-Optical Systems, Inc., U.S. Patent 3388291, "Annular Magnetic Hall Current Accelerator," patented June 11, 1968, filed August 31, 1964, Ser. No. 393288.

Curran, F. M. and Callahan, L. W., "The NASA On-Board Propulsion Program," AIAA-95-2379, July 1995.

Day, M. et al., "SPT-100 Subsystem Qualification Status," AIAA-95-2666, July 1995.

Garner, C. E., Brophy, J. R., Polk, J. E., Pless, L. C. and Starling, D. A., "A 5,730-Hr Cyclic Endurance Test of the SPT-100," IEPC-95-179, September 1995.

Gombosi, T. I., *Gaskinetic Theory*, Cambridge University Press, 1994.

Hamley, J. et al., "Development Status of the NSTAR Ion Propulsion System Power Processor," AIAA-95-2517, July 1995.

Lee, P. M. et al., "Similiarity Rule for Design of Linear Fluid Resistors and Its Application for Flow Measuring Problems," *Flow: Its Measurement and Control in Science and Industry*, Instrument Society of America, 1974.

Martin, D. L., "Prediction of Gas Flow Through Porous Plugs," *Flow: Its Measurement and Control in Science and Industry*, Instrument Society of America, 1974.

Shapiro, A. H., *The Dynamics and Thermodynamics of Compressible Fluid Flow*, Volumes 1 and 2, The Ronald Press Company, 1953.

Sutton, G. P., *Rocket Propulsion Elements*, John Wiley & Sons, Inc., 1992.

Zucrow, M. J. and Hoffman, J. D., *Gas Dynamics*, Volume I, John Wiley & Sons, Inc., 1976.

BIBLIOGRAPHY

Benedict, R. P. and Steltz, W. G., *Handbook of Generalized Gas Dynamics*, Plenum Press Data Division, 1966.

Bird, G. A., *Molecular Gas Dynamics*, Clarendon Press, 1976.

Davis, C. V. and Sorensen, K. E., *Handbook of Applied Hydraulics*, McGraw-Hill, 1969.

Emanuel, G., *Gasdynamics: Theory and Applications*, American Institute of Aeronautics and Astronautics, Inc., 1986.

Gilmore, D. G., *Satellite Thermal Control Handbook*, The Aerospace Corporation Press, 1994.

Holman, J. P., *Heat Transfer*, McGraw-Hill, 1990.

Keenan, J. H. et al., *Gas Tables*, John Wiley & Sons, Inc., 1948.

King, A. L., *Thermophysics*, W. H. Freeman and Company, 1962.

Kotake, S. and Hijikata, K., *Numerical Simulations of Heat Transfer and Fluid Flow on a Personal Computer*, Elsevier Science Publishers, 1993.

Mkhitaryan, A. M., *Hydraulics and Fundamentals of Gas Dynamics*, Israel Program for Scientific Translations, 1964.

Rawlin, V. K., "Power Throttling the NSTAR Thruster," AIAA-95-2515, July 1995.

Spores, R. A. et al., "The Air Force Electric Propulsion Program," AIAA-95-2378, July 1995.

Zucker, R. D., *Fundamentals of Gas Dynamics*, Matrix Publishers, Inc., 1977.

INITIAL DISTRIBUTION LIST

1. Defense Technical Information Center 2
   8725 John J. Kingman Road, Ste 0944
   Ft. Belvoir, Virginia 22060-6218

2. Dudley Knox Library 2
   Naval Postgraduate School
   411 Dyer Road
   Monterey, California 93943-5101

3. Chairman (Code AA) 1
   Department of Aeronautics and Astronautics
   Naval Postgraduate School
   Monterey, California 93943-5101

4. Dr. Oscar Biblarz (Code AA/Bi) 1
   Department of Aeronautics and Astronautics
   Naval Postgraduate School
   Monterey, California 93943-5000

5. Dr. Knox T. Millsaps (Code ME/Mi) 1
   Department of Mechanical Engineering
   Naval Postgraduate School
   Monterey, California 93943-5000

6. LT Dan A. Starling 2
   4304 Clarno Drive
   Austin, Texas 78749

7. Dr. John R. Brophy 3
   Jet Propulsion Laboratory
   California Institute of Technology
   Pasadena, California 91109

8. Mr. Craig Clauss 1
   Atlantic Research Corporation
   Liquid Propulsion Division
   5945 Wellington Road
   Gainesville, Virginia 22065